Surface Photometric Calibration of the Infrared Tully-Fisher Relation Using Cepheid-based Distances of Galaxies

Masaru Watanabe[1]
Japan Science and Technology Corporation, Tokyo 102-0081, Japan

Naoki Yasuda
National Astronomical Observatory of Japan, Tokyo 181-8588, Japan

Nobunari Itoh
Kiso Observatory, University of Tokyo, Nagano 397-0101, Japan

(*Submitted to Ap.J.*)

ABSTRACT

Infrared J and H surface photometry are carried out for nearby 12 galaxies whose distances have been accurately measured via HST Cepheid observations. Using the total, isophotal, and surface-photometric aperture magnitudes we calibrate the infrared luminosity-line width relation (IRTF). It is found that IRTF changes its slope at $\log W_{20}^c \sim 2.45$ in all the examined magnitude systems. The apparent scatter of IRTF is not significantly reduced when surface photometric magnitudes are used instead of the conventionally used synthetic aperture magnitude $H_{-0.5}$. It is also shown that the color $(I-H)_T$ of the nearby calibrator galaxies is redder by $\sim 0.2\,\mathrm{mag}$ than the Coma cluster galaxies, but such a trend is not clearly visible for the Ursa Major mostly because of poor statistics. The color offset of the Coma is analogous to that previously found in $I_T - H_{-0.5}$. From the present calibration of H-band IRTF, we obtain the distance to the Coma cluster to be $m - M = 34.94 \pm 0.13\,\mathrm{mag}$, where no account is taken of the $I - H$ color problem. Using the CMB-rest recession velocity of the Coma cluster we obtain $H_0 = 73 \pm 4\,\mathrm{km\,s^{-1}\,Mpc^{-1}}$.

Subject headings: galaxies: fundamental parameters — galaxies: photometry — galaxies: spiral — distance scale — infrared: galaxies

1. Introduction

The infrared luminosity-line width relation (hereafter IRTF) has been studied conventionally using the H-band synthetic aperture magnitude denoted as $H_{-0.5}$ (Aaronson et al 1986, Pierce & Tully 1988, Freedman 1990, Sakai et al 2000). Originally introduced by Aaronson, Mould & Huchra (1979), the $H_{-0.5}$ magnitude was defined as the flux observed within an aperture having a diameter $A = 10^{-0.5} D_{25}$, where D_{25} stands for the optical isophotal diameter measured at the surface brightness level of $\mu_B = 25\,\mathrm{mag\,arcsec^{-2}}$. Based on this rather heterogeneous magnitude system, the H-band IRTF has been a peculiar one compared

[1]Postal address: Center for planning and information systems, Institute of Space and Astronautical Science, Kanagawa 229-8510, Japan

with the optical TFs which are all based on the ordinary surface photometric magnitudes (e.g., Giovanelli et al. 1997b).

The $H_{-0.5}$ system was originally contrived from an observational limitation that a 2-D imager was not available in the infrared wavelength domain. Even after the advent of an infrared 2-D imager, its physical size had been insufficient for accurate surface photometry. In the meanwhile homogeneous data sets of $H_{-0.5}$ had been accumulated for both field and cluster galaxies (Aaronson et al. 1982, Bothun et al. 1985, Aaronson et al. 1989, Tormen & Burstein 1995 [hereafter TB95]). Because of their usefulness these data have played a pivotal role in the subsequent IRTF studies, and consequently led to the present paradigm of $H_{-0.5}$ system for IRTF studies. Nevertheless, it is also true that we still await IRTF to be calibrated with a surface photometric magnitude, as it provides a more fair and thus preferable measure of a galaxy luminosity. This requirement will be imminent and inflated as a significant progress will be made in extensive infrared surveys such as the 2-Micron All-Sky Survey (2MASS, Skrutskie et al. 1997) and the Deep Near-Infrared Southern Sky (DENIS) survey (Epchtein et al. 1994).

The infrared surface photometry of these galaxies is important not only for the calibration of the IRTF, but also for exploring the photometric properties of the nearby galaxies. Recently Sakai et al (2000; hereafter S00) has raised a question pertaining to the possible offset of the H magnitude between the nearby and cluster galaxies. In that paper they calibrated the luminosity-line width relations in $BVRIH_{-0.5}$ and applied them to 23 clusters to obtain the global value of H_0. From an internal comparison between H_0's obtained in these different wavelengths they found that the mean H_0 obtained in $H_{-0.5}$ is 10% smaller than those obtained in the others. Examining several observational properties of the sample galaxies they came to a conclusion that there should be a systematic difference in $H_{-0.5}$ between the nearby calibrators and the cluster galaxies. It is yet unclear, however, whether this difference somehow comes from this peculiar photometry technique of $H_{-0.5}$ or from a difference of intrinsic photometric properties between these galaxies. In order to disentangle this problem it is desirable to obtain surface photometry data for these nearby galaxies.

To address these issues we carry out J and H surface photometry for nearby galaxies having HST Cepheid distance measurements. These galaxies have a large apparent size of $3 - 10$ arcmin in diameter. Accurate imaging photometry of such large galaxies is made available with a large-format infrared camera attached to the Kiso Schmidt telescope (Itoh, Yanagisawa & Ichikawa 1995). With this configuration the camera covers an 18 arcmin-square field of view. Using the data we calibrate IRTF and apply the relation to cluster galaxies. Some H-band photometric properties of galaxies will be also examined including the H magnitude problem mentioned above.

Contents of this paper is as follows. Observations of the sample galaxies and literature data used are described in section 2. Photometry results, accuracy, and external consistency are presented in section 3. Calibration of IRTFs is given in section 4, followed by a discussion on photometric properties of the sample galaxies and the application of IRTF to cluster galaxies given in the literature in section 5.

2. The Sample and Observations

2.1. The Sample

Our sample comprises nearby 12 spirals (Table 1). They have been selected according to two criteria that HST Cepheid observations be available and that inclination be larger than 45° according to S00 or

RC3. The literature data of these galaxies are also summarized in Table 1. In order to be as consistent with S00 as possible, we refer to the compilation by S00 for all the external data including galaxy distances, H I line widths, and inclinations whenever available.

As for the extinction correction we adopt Schlegel et al (1998) for the Galactic extinction and Tully et al (1998) for the internal extinction. These were both adopted by S00 as well. Since Tully et al (1998) did not actually provide extinctions in J and H, these values are evaluated using relations $A_i^{(H)} = 0.5A_i^{(I)}$ given by S00 and $A_i^{(J)} = 0.8A_i^{(I)}$ obtained by ourselves from an interpolation between I and H. S00 does not include NGC 4639, therefore its H I line width data are taken from Huchtmeier & Richter (1989), and the inclination is computed using the axial ratio given in RC3 and the inclination formula given in S00.

As for the extinction corrections, there have been several alternative prescriptions advocated by different authors. To examine the effect of adopting different prescriptions we compare our adopting A_g and A_i with those computed from Burstein & Heiles (1984) and RC3, respectively. Note in advance that since the uncertainty in the absolute magnitudes of galaxies due to the distance error is already more than 0.1 mag, that due to differences in various extinction correction methods is negligible. The Galactic extinction by Burstein & Heiles (1984) is presented in B hence converted to those in J and H using the ratio of $A_g^{(B)} : A_g^{(J)} : A_g^{(H)} = 4.315 : 0.902 : 0.576$ given by Schlegel et al (1998). This comparison shows that the Burstein's value is systematically different from our A_g only by less than 0.02 mag, which is of no significance in the present study. For the comparison of the internal extinction the B-band value given in RC3 is also converted to those in J and H. In this conversion we are based on the ratio given by Tully et al (1998). They provide $A_i^{(I)}/A_i^{(B)} = 0.59$ which, in conjunction with the above-mentioned relations between $A_i^{(I)}$, $A_i^{(J)}$, and $A_i^{(H)}$, leads to a ratio of $A_i^{(B)} : A_i^{(J)} : A_i^{(H)} = 1 : 0.47 : 0.30$. This ratio is substantially different from that previously given for A_g. According to Han (1992) and Tully et al (1998), this difference is mostly ascribed to the configurations of the Galactic and internal extinction which compel a light ray to pass through a different path lengths toward us. From this conversion it is shown that the systematic difference of A_i between RC3 and our adopted scheme is mostly less than 0.05 mag, except for only NGC 7331 which raises 0.1 mag difference. These differences are again negligible in the present work. As emphasized in S00, which scheme to choose is insignificant but a consistency is important in a TF analysis.

2.2. Observations

The J and H images were obtained using the 105cm Schmidt telescope at the Kiso Observatory during the period between 1998 October and 1999 October. Because of a time limitation a J image of NGC 4536 could not be obtained. The telescope was equipped with a large-format near-infrared camera called the Kiso Observatory Near Infrared Camera or KONIC as abbreviated (Itoh, Yanagisawa & Ichikawa 1995). KONIC is a PtSi camera having 1040×1040 physical pixels. The output data are binned into 1040×520 pixels, while we use the image further binned into 520x520 pixels. The camera mounted on the Kiso Schmidt covers 18 arcmin-square FOV hence has a pixel scale of 2.12 arcsec par the 2×2 binned pixels.

A single on-source exposure for a targe galaxy was taken to be 300 sec. The same duration was assigned to an off-source exposure for a blank sky region displaced by at least 20 arcmin from the target galaxy. The off-source exposure was taken after every 2 on-source exposures. Typically successive 12 on-source exposures plus 6 intervening off-source exposures were thus taken for a single galaxy. The number of the on-source exposures actually varied from 4 to 16 depending on the galaxy brightness and/or a sky condition of the night. Along with these exposures, infrared standard stars of Elias et al (1982) were also observed

every night at various zenith distances for the magnitude calibration. The exposures for the standard stars were appropriately defocused so that we could accumulate a sufficient number of the background signal count to avoid a deferred charge problem of the camera (Itoh, Yanagisawa & Ichikawa 1995).

2.3. Data reduction

The observed data were reduced using an image reduction software IRAF[2] V2.11.3 and STSDAS V2.1. A dark count was estimated and subtracted from the raw image using the Richardson's formula calibrated with the dark images. Image flattening was performed in a usual manner using combined blank sky images. A reduction error in these procedures are discussed later in section 3.2. A sky background region in the galaxy frame was determined as an exterior region of a circle centered at the target galaxy. The radius, which extended up to $\sim 7\,$arcmin for the largest galaxies such as NGC 925, 4725, and 7331, was determined according to the apparent size of the galaxy. Signal counts of the sky background region was fitted with polynomial surfaces of several orders, and the best one determined by the visual inspection into the residual counts was subtracted from the image. Actually a first-order polynomial surface was sufficient for most of the images. The remaining signal counts were then corrected for the atmospheric extinction and converted into the count in the CIT magnitude system using the standard star data reduced in a similar way. In this conversion the extinction coefficients were determined for each individual night separately while the color conversion coefficients were commonly taken from the recommended color equations $J_{Kiso} = J_{CIT} + 0.06(J-H)_{CIT}$ and $H_{Kiso} = H_{CIT} + 0.10(J-H)_{CIT}$.

Considering an undesirably extended psf of the camera (Yanagisawa, Itoh & Ichikawa 1996) we deconvolved the galaxy images using a psf image. The deconvolution was performed using the Lucy-Richardson's method realized in the STSDAS package. In this deconvolution two different psf images were separately applied to the same galaxy images to see an internal consistency. One psf is composed with several undisturbed stellar images in a galaxy frame, while the other is taken from a template psf image created earlier for an instrumental verification purpose. Each of the psfs has its own advantage over the other; the former has the same seeing condition as have the galaxy image to be working on, while the latter has a sufficiently high S/N hence reproduces the extended fainter outskirt of the psf more clearly. Performing these two deconvolutions we obtained alternative results, i.e., the former experiment reproduces the galaxy aperture data which are in better agreement with the literature data as used in section 3.3.1 while the latter provides better rectification of galaxy images without any discernible psf outskirt even around bright galaxies. The worse agreement of the aperture data for the latter deconvolution experiment is that the deconvolved galaxy image provides systematically too bright a magnitude at the inner apertures. It is noted that this systematic discrepancy, amounting typically to $\sim 0.1\,$mag, is unlikely due to a difference of the seeing disk conditions between our observations and those for the aperture photometry of the literature data; this is because the discrepancy remains up to an aperture whose diameter is a few tens of seconds, where the difference of the seeing size should be no more an important issue on the aperture magnitude.

In spite that these two experiments of deconvolution provide partly unsatisfactory results, they nevertheless give consistent results regarding global photometry parameters such as the total, isophotal, and, synthetic aperture magnitudes that we are mostly concerned with in this study. Making best use of this preferable result, we constructed a moderate psf image merging the kernel of the former psf and

---

[2]IRAF is distributed by the National Optical Astronomy Observatories, which is operated by the Association of Universities for Research in Astronomy, Inc. (AURA) under cooperative agreement with the National Science Foundation.

the extended cross and ring-like pattern of the latter. We find that the composite psf provides the most satisfactory deconvolution result in the sense that it simultaneously reduces the two undesirable aspects of the previous deconvolutions. Accordingly, the composite psf was created for and applied to each individual galaxy for the deconvolution.

After the deconvolution foreground stellar images were cleaned out using the interpolation from the surrounding sky background count to provide the final galaxy image for photometry. None of the foreground stars severely contaminates the target galaxies, thereby we may disregard any photometry uncertainty to be introduced in this cleaning procedure. The deconvolution often generated a ring-shaped negative overshoot around bright stars. The amplitude of the overshoot was however negligible compared with the gross internal photometry error, so these defects were just cleaned in the same light of cleaning the inner stellar image.

The amplitude of the sky background shot noise is typically equivalent to the surface brightness levels of $\mu_J = 21\,\mathrm{mag\,arcsec^{-2}}$ and $\mu_H = 20\,\mathrm{mag\,arcsec^{-2}}$. In order to increase S/N of the fainter part of the galaxies we smoothed the image using a 5 pixel-square or 11 arcsec-square boxcar window. On the smoothed image we computed a series of isophotes at various surface brightness levels and fitted ellipses to the isophotes. The luminosity profiles and contour maps are given in Fig.1. We compute several isophotal parameters at $\mu_J = 22\,\mathrm{mag\,arcsec^{-2}}$ and $\mu_H = 21\,\mathrm{mag\,arcsec^{-2}}$, which are collectively presented later in section 3. A caution is needed for the map of NGC 925 in J, as the isophotes is less reliable at its north-eastern outskirts. That portion of the image is unfortunately disturbed by a deferred charge in some pixel rows proximity to the overscan area attached to the boundaries of each quadrant of the detector array. This degradation of the image may affect the accuracy of some isophotal geometrical parameters. However, the fraction of the disturbed light is quite small compared with the galaxy total light, so we presume that the J photometry of NGC 925 does not suffer any additional serious uncertainty from this peripheral image degradation.

To obtain asymptotic total magnitudes J_T and H_T we extrapolated the exponential disk to infinity. In this extrapolation the disk part of the galaxies was determined from the visual inspection into the luminosity profiles. To verify this determination we also referred to the axial ratio and the position angle varying along with the isophotal radius. The extrapolation typically amounts to 0.05 mag with a few exception of faint or short exposure galaxies for which we need $0.2 - 0.3$ mag of extrapolation. The extrapolation is subject to the uncertainties of the axial ratio, disk scale length, and central surface brightness adopted for the exponential disk. The error is assessed later in section 3.2 as a source of a photometry error for J_T and H_T.

3. Surface photometry data

3.1. Data presentation

The results of the surface photometry are summarized in Table 2. Description of the columns are as follows; column(1) NGC number, column(2) Asymptotic total magnitude J_T and its error, column(3) Isophotal magnitude J_{22} and its error, column(4) Isophotal major axis length D_{J22} in arcmin, column(5) Effective radius $r_e^{(J)}$ in arcmin, column(6) Minor-to-major axial ratio R_{J22}, column(7) Asymptotic total magnitude H_T and its error, column(8) Surface photometric aperture magnitude $H^s_{-0.5}$ with the modified aperture of TB95, and its error, column(9) Isophotal magnitude H_{19} and its error, column(10) Isophotal magnitude H_{21} and its error, column(11) Isophotal major axis length D_{H19} in arcmin, column(12) Isophotal major axis length D_{H21} in arcmin, column(13) Effective radius $r_e^{(H)}$ in arcmin, column(14) Minor-to-major axial ratio R_{H21}. Derivation of the quoted photometry error is discussed in the subsequent section. The

nominal disagreement between R_{J22} and R_{H21} is mostly ascribed to the measurement uncertainty; it is evaluated to be ~ 0.05 based on their scatter within the surface brightness levels of $\mu_J = 22\,\mathrm{mag\,arcsec^{-2}}$ and of $\mu_H = 21\,\mathrm{mag\,arcsec^{-2}}$.

3.2. Photometric Accuracy

3.2.1. Internal photometry error

Sources of the internal photometry error differ between the asymptotic, isophotal, and aperture magnitudes. For the asymptotic magnitude J_T and H_T the error Δ is estimated as $\Delta^2 = \Delta_{flt}^2 + \Delta_{clb}^2 + \Delta_{ext}^2$ where Δ_{flt}, Δ_{clb}, and Δ_{ext} represent the errors caused by the flattening procedure, magnitude calibration procedure, and the disk extrapolation procedure, respectively. For the remaining magnitudes such as J_{22}, H_{19}, H_{21}, and $H_{-0.5}^s$ the internal error should be $\Delta^2 = \Delta_{flt}^2 + \Delta_{clb}^2$. Each of these error sources is described in what follows.

Flattening We computed a dark count of an object frame using the Richardson's formula calibrated with the data taken from a number of dark frames. The scatter of the data around the fitted formula is typically 10 ADU. A signal count of a single sky flat frame of a 300 sec exposure was, on the other hand, generally larger than 2000 ADU/pixel in J and 5000 ADU/pixel in H excluding the bias and dark counts. Accordingly, the 10 ADC error of the dark count subtraction causes flattening errors less than 0.5 % and 0.2 % in J and H, respectively. A more serious error in the flattening procedure is brought by a temporal variation of a local sky background brightness. To examine this variation we divided the associated off-source sky background images each other and see the distribution of the data counts in the quotient frame. From this examination no discernible global gradient of the sky background count is found for all the associated sky frames. A discernible deviation from the mean count is of rather random nature. The fractional deviation amounts to 3 % at most both in J and H at the central part of the frames where a target galaxy was always exposed. As the deviation is for a single object frame, we summed it up quadratically for all the combined galaxy frames. From this, we obtain the uncertainty to be 1.5 % for a combination of 4 frames (1200 sec exposure, the shortest in the present observations) and 0.8 % for a composition of 16 frames (4800 sec exposure, the longest).

Extrapolation of the exponential disk Extrapolation of the exponential disk is parameterized by the disk scale length, disk central surface brightness, and the axial ratio. The former two components are derived from a linear fit to the luminosity profile, while the axial ratio is taken from S00. Adoption of this axial ratio is because the optical isophote refers to a deeper surface brightness level and because we like to avoid a possible unknown systematic error that may be introduced in our axial ratio through the deconvolution procedure. We computed the extrapolation error by practically changing these parameters within a reasonable range. The error is obtained to be $0.03 - 0.10$ mag depending on the apparent brightness of the galaxies.

Magnitude calibration The magnitude calibration error is estimated as the scatter of the standard star data around the equation of atmospheric extinction correction and color transformation. The scatter is typically 0.03 mag.

Taking all the errors given above into account we evaluate the internal photometry error for individual galaxies. The value is given for each magnitude in Table 2. We achieve a typical accuracy of 0.06 mag for the total magnitude except for two faintest galaxies NGC 2541 and 3319. The accuracy is even better for aperture and isophotal magnitudes as they refer only to relatively brighter portion of the galaxy image.

3.3. External consistency

3.3.1. Photometry

Growth curves of each galaxy are computed using a series of circular apertures. We compare the curves with aperture photometry data given in the literature to check an external consistency. The literature data include Glass (1976), Aaronson (1977), Peletier & Willner (1991), TB95, and the 2MASS extended source catalog available on the web (http://irsa.ipac. caltech.edu/applications/CatScan/).

The result of the comparison is shown in Fig.2. Most of the literature data show an agreement with our values within 0.1 mag. A relatively large and systematic discrepancy worth mentioning is observed in the following four galaxies; NGC 3198 : Aperture data of TB95 (2 apertures) are systematically fainter by 0.15 mag than our photometry. NGC 3319 : Aperture data of TB95 (3 apertures) are systematically fainter by 0.1 mag than our photometry. NGC 4639 : We find an increasing discrepancy toward larger apertures between surface photometric aperture data of 2MASS (9 apertures) and ours. The discrepancy amounts to ~ 0.3 mag at the outermost aperture. Aperture data of Peletier & Willner (1991) (1 aperture) are more consistent with the 2MASS data sequence. On the other hand, the template curve of TB95 for this type of galaxy ($T = 4$) matches better with our growth curve at the outer slope, implying that the 2MASS photometry is not sufficiently deep for this galaxy. NGC 4725 : Aperture data in H by TB95 (5 apertures) are fainter by 0.1 mag than our photometry. As for these four galaxies, independent data are needed to give further discussion on this photometry result. There are two other galaxies which show large discrepancy regarding $H_{-0.5}$; NGC 4535 : $H_{-0.5}$ of TB95 is fainter by 0.29 mag than our $H^s_{-0.5}$. This error on $H_{-0.5}$ is ascribed to its wavy growth curve which cannot be well fitted with the monotonically increasing template curve of TB95. NGC 7331 : $H_{-0.5}$ of TB95 is brighter by 0.36 mag than our $H^s_{-0.5}$. This error on $H_{-0.5}$ is attributed to the lack of aperture data having a larger diameter.

3.3.2. Axial ratio

We compare the axial ratio with those obtained by S00. The agreement is better than $\Delta R = 0.05$ for most of the galaxies. Relatively large error is found for NGC 3319 ($R_{J22} = 0.37$ and $R_{H21} = 0.32$, while $R_{S00} = 0.51$). The compilation of the kinematical inclinations by S00 indicate $R = 0.53$, which is in better agreement with R_{S00}. This large discrepancy of the axial ratio of NGC 3319 is ascribed to its faint, loosely-wound spiral arms. In the infrared images these arms are hardly visible, therefore they give negligible contribution to determining the axial ratio. This suggests that the optical image is generally perferable for determining the inclination of spirals.

4. Calibration of the infrared luminosity-line width relations

IRTF diagrams calibrated in several magnitudes are shown in Fig.3. A striking feature common to all of the diagrams is that the IRTF changes its slope at around $\log W_{20}^c \sim 2.45$. A further discussion on this issue is given in the subsequent section using an enlarged sample. Results of the linear regression fit characterized by the slope, zero point, and the apparent scatter, are summarized in Table 3. These parameters are computed both for the entire sample and for the subsample limited to $\log W_{20}^c > 2.45$. Note a considerable reduction of the apparent scatter for the subsample compared with that of the entire sample.

The calibration result with $H_{-0.5}^s$ is apparently in good agreement in slope, zero point, and apparent scatter compared with that obtained by S00. It should be noted that S00 referred to Aaronson et al (1982) for the synthetic aperture photometry scheme which is different in the aperture system and the growth curve templates from the TB95 scheme that we adopt for $H_{-0.5}^s$. Accordingly, the present agreement implies that the photometry schemes of Aaronson et al (1982) and TB95 have been both adequately accurate to obtain $H_{-0.5}$ for the purpose of applying it to IRTF, given the current uncertainty of other observables such as the line width, inclination, and extinctions.

5. Discussion

In this section we add Coma cluster data by Bernstein et al (1994) and Ursa Major (UMa) cluster data by Peletier & Willner (1993) to the discussion in order to enlarge the sample and to apply the present calibration result to. Both of the photometry data were calibrated using the Elias's standard stars hence have a zero point comparable with our data. Bernstein et al (1994) provided H_T for 21 galaxies, among which 12 galaxies are also given $H_{-0.5}$ by TB95. Galaxy inclination and H I line width data are taken from their original measurement and compilation. Peletier & Willner (1993) provides H_T, $H_{-0.5}^s$ and H_{19} for 22 galaxies. Inclination and the line width are taken from their paper. Corrections for the Galactic and internal extinctions are performed following the manner we applied to the present sample.

5.1. Photometric properties of $H_{-0.5}$

We first examine the difference between TB95's aperture magnitude, $H_{-0.5}$ and our $H_{-0.5}^s$ as a function of a galaxy inclination and of type to see any systematic errors in $H_{-0.5}$. They both show no significant dependency, which means that the error of $H_{-0.5}$ predominantly comes from a random error.

We examine dependencies of $H_{-0.5} - H_T$ on a galaxy axial ratio and on type (Fig.4). Neither early nor late spirals exhibit a significant dependency of $H_{-0.5}^s - H_T$ on the axial ratio. As is qualitatively expected from the variety of the bulge-to-disk light ratio on galaxy types, the mean values of $H_{-0.5}^s - H_T$ is different between these two type ranges; $H_{-0.5}^s - H_T = 0.62 \pm 0.05$ mag for $T \leq 4$ while $H_{-0.5}^s - H_T = 0.77 \pm 0.06$ mag for $T \geq 5$. This difference implies that the application of IRTF in $H_{-0.5}$ need a caution; if the calibrators and the cluster samples consist of considerably different population in terms of galaxy types, these may lead to a distance estimate suffering from a systematic error.

A rather curious implication from this data plot is a deficiency of late spirals with $H_{-0.5}^s - H_T > 0.5$ at $0.3 < D_{min}/D_{maj} < 0.5$. We are yet to be confident of its reality, however, and certainly think that we need much more data for any further discussion. If this ever turns out to be the case, the rather moderate range of the axial ratio will make it an interesting and challenging problem.

5.2. Environmental dependence of galaxy color

S00 demonstrated that there is a significant discrepancy between H_0's obtained in I and $H_{-0.5}$ which corresponds to a systematic difference by 20% of the sample cluster distances. In a close relation to this it is also shown in S00 that the nearby calibrators have a redder color in $I_T - H_{-0.5}$ (but not in $(B-I)_T$) than the Virgo, Ursa Major, Coma, and two other clusters for a fixed $\log W_{20}^c$. We confirm that this $I_T - H_{-0.5}$ color offset persists even if we use $H_{-0.5}^s$ for the nearby calibrators. Instead of $I_T - H_{-0.5}$, we plot $(I-H)_T$ in Fig.5. Although the Ursa Major galaxies show a relatively wide distribution regardless of $\log W_{20}^c$ and the sample seems yet poor, the plot for the Coma galaxies shows with more convinction that the nearby calibrators are likely redder than the cluster galaxies. This fact indicates that some intrinsic color offset really exists in $I-H$ between the nearby calibrators and a certain cluster of galaxies. To see whether this color offset is caused alone by the possible peculiar properties of the H luminosity, we plot another color $(B-H)_T$ in Fig.6. In this figure nearby calibrators are again found to be redder than the Coma galaxies but not so compared with the UMa. These experiments demonstrate that, although the color offset in $I-H$ is quite likely to be real, we may not come to a hasty conclusion that the nearby calibrators are always redder than cluster galaxies in the colors relevant to H. To address this color problem further in detail we need to accumulate more H photometry data and examine the relevant colors reflecting the cluster environment.

5.3. Implication of properties of IRTF

Whether the TF relation is linear for a respectable range of the line width or not has been an issue of controversy; while most of the TF studies have assumed a linearity in TF relation, some studies (e.g., Aaronson et al 1986; Mould, Han & Bothun 1989; McGaugh et al 2000) adopted or argued for the nonlinearity of the relation.

As shown in Fig.3, our result of IRTF calibration apparently exhibits a breakdown for fainter galaxies with $\log W_{20}^c < 2.45$ regardless of the bandpass or magnitude system. This boundary may be comparable with a similar break at $V_c(\sim W_{20}^c) \sim 90\,\mathrm{km\,s^{-1}}$ demonstrated by McGaugh et al (2000). The IRTF diagrams for the Ursa Major clusters are shown in Fig.7, where the apparent magnitude is used instead. Overplotted are the IRTFs of the nearby calibrators as shown in Fig.3 but vertically scaled so that the gross scatter be minimized at the range $\log W_{20}^c \geq 2.45$. Note in passing that this procedure yields simultaneously the cluster distance and the slope of the IRTF for the composite sample of galaxies, to which we will be back in the next section. It is evident from these diagrams that the breakdown of IRTF is reproduced by the UMa galaxies. Note also that the distribution of nearby calibrators and the cluster galaxies for $\log W_{20}^c < 2.45$ are naturally homogenized as well. Although the sample is not definitive yet, these facts provide another support to that the breakdown is a common features of IRTF irrespective of galaxy environment. It should be noted, however, that the distribution of these fainter galaxies exhibits a larger scatter and a steeper slope which render a separate linear fitting to these data almost meaningless compared with the brighter galaxies with $\log W_{20}^c > 2.45$. This suggests that, when IRTF is used for measuring extragalactic distance scale, these intrinsically fainter galaxies should be excluded from the fitting procedure so as not to introduce unnecessary systematic error to the inferred distance.

In spite that the photometry error is now reduced down to < 0.1 mag which is negligible compared with the apparent scatter of the TF relation, we do not obtain a significant reduction of the apparent scatter by using the H_T instead of $H_{-0.5}^s$ (Table 3). This suggests that the apparent scatter has no more

been dominated by the uncertainty of the photometry, but rather by the errors of the distance and intrinsic line width estimates, or else by the intrinsic scatter itself. Since it is currently practically difficult to obtain a more accurate distance for the calibrators, reducing the line width error seems to be the most feasible and promising strategy to take to approach the intrinsic shape of IRTF. To achieve a successful result with this strategy, we need to obtain, among other things, definitive numbers for the inclination of the nearby calibrators.

5.4. Distances to UMa and Coma clusters and H_0

Taking tentatively no account of the color problem discussed in the previous section, we give an estimate of the cluster distances based on the present IRTF calibrations. IRTF diagrams for the Coma cluster galaxies is shown in Fig.8. Nearby calibrators are overplotted, and the distance and the slope of IRTF for the composite sample are obtained in the same manner as described for UMa galaxies in Fig.7. In what follows the distances (and the slopes) are derived from only galaxies with $\log W_{20}^c \geq 2.45$ because of the reason discussed in section 5.3. This limitation takes an extra advantage for especially the distant Coma sample since a sample incompleteness bias becomes almost negligible for the brighter galaxies (Giovanelli et al 1997b).

Estimates of the distance modulus of the UMa and Coma are summarized in Table.4. The quoted error is evaluated as a square root of the sum of the squares of dispersions around the calibrated IRTF and the cluster IRTF each divided by the respective number of galaxies. For UMa the distance estimates in H_T, $H_{-0.5}$, and H_{19} show an excellent agreement each other, as well as with that obtained by S00 in I, $m - M = 31.58$ mag. This agreement with the distance in I seems inconsistent with S00's implication that there is a severe $I - H$ offset between UMa galaxies and the nearby calibrators. However, our examination of the $I - H$ color using H_T has not provided definitely such a color offset for UMa galaxies yet (Fig.5).

Estimates of the Coma cluster distance in H_T and $H_{-0.5}$ exhibit a nominal discrepancy amounting to 0.11 mag. Although this is within the quoted error, we find that this discrepancy is ascribed to this particular Coma sample for $H_{-0.5}$. This is evident from the left panel of Fig.8, where it is illustrated that the majority of the galaxies with $H_{-0.5}$ data are located underneath the regression line line of the IRTF in H_T. Indeed, if the H_T sample is biased analogous to the $H_{-0.5}$ sample, i.e., limited to those with $H_{-0.5}$ measurements available, the distance modulus of Coma in H_T is increased up to $m - M = 35.08$ mag (the fourth row in Table.4), which is consistent with the biased distance inferred in $H_{-0.5}$.

It is worth commenting that this tendency found for the $H_{-0.5}$ subsample of Coma is also observed in the TF diagram in I_T, i.e., Coma galaxies with $H_{-0.5}$ measurements available tend to be found below the mean regression line in I_T. This was assured by identifying $H_{-0.5}$-measured galaxies (Bothun et al 1985) in Giovanelli et al (1997a)'s sample and drawing the TF diagram in I_T. Similar identification and check were carried out for ACO 1367, 2634, 400, NGC 383 group, NGC 507 group, Cancer, and Pegasus, but such a trend was not observed in these samples.

We see a shallower slope of -5.66 for the H_T sample of UMa. This should be apparently ascribed to NGC 3718 which has a largest deviation in H_T among the UMa galaxies. Peletier & Willner (1993) found the similar deviation for this galaxy and argued a plausible reason, in terms of its optical morphological peculiarity, of justifying its exclusion from the TF sample.

We see in Fig.4 that there is a type dependence in $H_{-0.5} - H_T$. Although a KS test suggests no

significant difference (at a $> 70\%$ confidence level) of the morphological type distribution between the calibrators, Coma galaxies, and UMa galaxies, we examine the galaxy type dependence of the distance estimates. We divide the cluster galaxies into two subsamples of $T \leq 4$ and $T \geq 5$ and estimate the cluster distances separately using these subsamples and nearby calibrators divided into two as well. The result is shown in the fifth and sixth rows in Table.4. For UMa galaxies the result is consistent with that obtained from the entire analysis. For Coma galaxies, we obtain a nominally shorter distance $m - M = 34.70$, nevertheless it is still consistent with the global value if we consider the large error associated to this poor statistics.

We adopt the distance modulus $m - M = 34.94\,\mathrm{mag}$ obtained in H_T as our best estimate of the Coma distance. This number, compared with $m - M = 34.74\,\mathrm{mag}$ obtained by S00 in I, is larger by $0.2\,\mathrm{mag}$. This discrepancy is less than 2σ confidence level from our error budget. However, being consistent with what is expected from the $I - H$ color problem discussed in the previous section, this discrepancy may not be considered as an error of a random origin.

Using $m - M = 34.94\,\mathrm{mag}$ of the Coma cluster and the recession velocity of $V = 7143\,\mathrm{km\,s^{-1}}$ in the CMB reference frame, and assuming that the deviation from the Hubble flow is negligible, we obtain $H_0 = 73 \pm 4\,\mathrm{km\,s^{-1}\,Mpc^{-1}}$. This value is nominally consistent with the global value of H_0 concluded by S00.

6. Summary

Infrared J and H surface photometry have been carried out for 12 galaxies having a Cepheid distance available via HST observations. Using the data we have calibrated IRTFs in the J- and H-bands. Photometric properties of $H_{-0.5}$ and colors relevant to H have been examined. The calibrated IRTFs are applied to the Coma and Ursa Major galaxies.

The main results we have obtained are as follows;

(1) The surface photometry results are given in Table 2. Calibrations of J and H IRTFs are summarized in Table 3.

(2) The offset of $H_{-0.5}$ from H_T shows no significant dependence on the galaxy axial ratio. It is galaxy-type dependent such that $H_{-0.5} - H_T$ is larger by $0.15\,\mathrm{mag}$ for late type spirals ($T >= 5$) than early ones ($T <= 4$).

(3) The nearby calibrators are redder in $(I - H)_T$ than the Coma galaxies. This is analogous to the property in $I_T - H_{-0.5}$ claimed by S00, but such a trend is not clearly visible for UMa mostly because of poor statistics. It is yet unclear whether the color offset is caused alone by any peculiarity of the H luminosity.

(4) It is shown in all the magnitude systems that the IRTF changes its slope at $\log W_{20}^{c} \sim 2.45$. This phenomenon is observed for the Ursa Major galaxies as well. The apparent scatter is not significantly improved even if we use surface photometric magnitudes instead of $H_{-0.5}$.

(5) From the application of the present calibration of IRTF to the Coma cluster, we obtain its distance to be $m - M = 34.94 \pm 0.13\,\mathrm{mag}$. With its CMB-rest recession velocity we obtain $H_0 = 73 \pm 4\,\mathrm{km\,s^{-1}\,Mpc^{-1}}$. It should be noted here that the distance is given no account of the possible color offset mentioned in (4) hence can be overestimated by $\sim 0.2\,\mathrm{mag}$.

We are deeply indebted to Takashi Ichikawa and Kenshi Yanagisawa for their lengthy efforts to develop and improve the large-format infrared camera KONIC to be available on the Kiso Schmidt. Kenshi Yanagisawa has kindly provided us with a psf image of KONIC. Thanks are due to the staff members of the Kiso Observatory for their technical supports during the observations. The literature data used in this study was made available in the electronic form from the Astronomical Data Analysis Center at National Astronomical Observatory of Japan. We thank the referee for many valuable comments which improved the manuscript.

Table 1. Sample galaxies and literature data

NGC	$m - M$ [mag]	Type[(a)]	D_{25}[(a)] [arcmin]	i[(b)]	$\log W^c_{20}$[(b)] [$\mathrm{km\,s^{-1}}$]	$A^{(J)}_{G+i}$[(c)] [mag]	$A^{(H)}_{G+i}$[(c)] [mag]
925	29.84 (.08)[(1)]	7	10.47	56	2.420	0.22	0.14
2541	30.47 (.08)[(2)]	6	6.31	62	2.370	0.22	0.14
3198	30.80 (.06)[(3)]	5	8.51	68	2.531	0.32	0.21
3319	30.78 (.12)[(4)]	6	6.17	58	2.405	0.17	0.11
3351	30.01 (.08)[(5)]	3	7.41	45	2.586	0.14	0.10
3368	30.20 (.10)[(6)]	2	7.59	49	2.674	0.19	0.11
4414	31.41 (.10)[(7)]	5	3.63	46	2.743	0.30	0.19
4535	31.10 (.07)[(8)]	5	7.08	51	2.586	0.19	0.11
4536	30.95 (.08)[(9)]	4	7.59	69	2.562	0.36	0.23
4639	32.03 (.22)[(10)]	4	2.75	49[(a)]	2.619[(a)]	0.18	0.11
4725	30.57 (.08)[(11)]	2	10.72	62	2.671	0.15	0.10
7331	30.89 (.10)[(12)]	3	10.47	69	2.746	0.50	0.31

The error of $m - M$ is given in parentheses.

[(a)]From RC3

[(b)]From Sakai et al (2000) except for NGC 4639 which is taken from Huchtmeier & Richter (1989) for $\log W^c_{20}$ and from RC3 for i.

[(c)]From Schlegel et al (1998) for the Galactic extinction A_G and Tully et al (1998) for the internal extinction A_i. See text for details.

References for $m - M$ — (1)Silbermann et al. 1996, (2)Ferrarese et al. 1998, (3)Kelson et al. 1999, (4)Sakai et al. 1999, (5)Graham et al. 1997, (6)Tanvir et al. 1995, (7)Turner et al. 1998, (8)Macri et al. 1999, (9)Saha et al. 1996, (10)Saha et al. 1997, (11)Gibson et al. 1999, (12)Hughes et al. 1998

Table 2. Photometry result

NGC	J_T	J_{22}	D_{J22}	$r_e^{(J)}$	R_{J22}	H_T	$H^s_{-0.5}$	H_{19}	H_{21}	D_{H19}	D_{H21}	$r_e^{(H)}$	R_{H21}
925	8.47 (.06)	8.82 (.03)	6.24	3.10	.55	7.54 (.05)	8.34 (.02)	9.90 (.02)	8.03 (.02)	1.51	6.48	3.80	.54
2541	10.30 (.11)	10.78 (.03)	2.95	1.75	.52	9.85 (.11)	10.34 (.02)	12.47 (.02)	10.43 (.02)	0.40	2.41	1.47	.47
3198	8.71 (.06)	8.83 (.03)	6.06	1.73	.33	7.93 (.05)	8.39 (.02)	8.80 (.02)	8.16 (.02)	2.68	5.57	1.93	.34
3319	9.91 (.11)	10.48 (.03)	4.12	2.50	.37	9.15 (.11)	10.25 (.02)	12.27 (.02)	10.07 (.02)	0.62	3.65	2.73	.32
3351	7.39 (.06)	7.51 (.03)	6.99	2.23	.76	6.90 (.05)	7.37 (.02)	7.39 (.02)	6.96 (.02)	2.50	5.81	1.73	.70
3368	6.97 (.05)	7.06 (.02)	7.51	1.68	.69	6.24 (.05)	6.75 (.02)	6.71 (.02)	6.33 (.02)	3.12	7.46	1.73	.70
4414	7.78 (.05)	7.84 (.02)	4.51	1.02	.76	7.14 (.05)	7.70 (.02)	7.41 (.02)	7.23 (.02)	2.30	3.91	0.90	.67
4535	7.81 (.05)	8.03 (.02)	6.34	2.81	.74	7.31 (.06)	8.33 (.03)	8.50 (.03)	7.62 (.03)	2.27	5.56	2.77	.68
4536	···	···	···	···	···	7.52 (.05)	8.14 (.02)	8.44 (.02)	7.79 (.02)	2.09	6.44	1.93	.39
4639	9.34 (.06)	9.46 (.03)	2.77	0.79	.67	8.56 (.05)	9.26 (.02)	9.10 (.02)	8.69 (.02)	1.19	2.71	0.83	.74
4725	7.13 (.05)	7.24 (.02)	8.79	2.69	.53	6.21 (.05)	6.88 (.02)	6.88 (.02)	6.39 (.02)	4.69	8.93	3.10	.58
7331	6.88 (.05)	6.95 (.02)	8.49	1.43	.46	6.15 (.05)	6.42 (.02)	6.53 (.02)	6.29 (.02)	3.67	7.40	1.50	.52

See text for column definitions.

Table 3. IRTF Calibration Result

Mag.	N	Slope	Zero point	Apparent scatter
H_T (all)	12	-9.84 (.36)	-22.59 (.23)	0.38
H_T ($\log W^c_{20} > 2.45$)	9	-7.54 (.76)	-22.95 (.35)	0.28
$H^s_{-0.5}$ (all)	12	-10.64 (.34)	-21.93 (.22)	0.36
$H^s_{-0.5}$ ($\log W^c_{20} > 2.45$)	9	-8.37 (.72)	-22.29 (.34)	0.29
H_{21} (all)	12	-11.57 (.34)	-22.15 (.22)	0.40
H_{21} ($\log W^c_{20} > 2.45$)	9	-8.14 (.71)	-22.70 (.34)	0.22
H_{19} ($\log W^c_{20} > 2.45$)	9	-10.24 (.72)	-21.95 (.34)	0.15
J_T (all)	11	-9.67 (.36)	-21.93 (.23)	0.32
J_T ($\log W^c_{20} > 2.45$)	8	-8.48 (.85)	-22.13 (.39)	0.30
J_{22} (all)	11	-10.95 (.34)	-21.61 (.23)	0.34
J_{22} ($\log W^c_{20} > 2.45$)	8	-8.87 (.82)	-21.97 (.38)	0.28

The error is given in parentheses.

Table 4. Distance modulus to clusters

Mag.	Coma				UMa			
	$m-M$	Slope	σ	N	$m-M$	Slope	σ	N
H_T	34.94 (.13)	-7.24	0.28	20	31.57 (.14)	-5.66	0.33	15
$H_{-0.5}$	35.05 (.14)	-7.67	0.28	11	31.56 (.14)	-7.44	0.31	15
H_{19}	···	···	···	···	31.56 (.14)	-8.22	0.41	15
H_T($H_{-0.5}$ avail.)	35.08 (.14)	-7.53	0.26	11	···	···	···	···
$H_T(T \le 4)$	34.70 (.20)	-6.08	0.27	7	31.59 (.17)	-5.71	0.36	9
$H_T(T \ge 5)$	35.08 (.16)	-7.87	0.25	4	31.55 (.18)	-5.43	0.29	6

The samples include only galaxies with $\log W^c_{20} \ge 2.45$. The Coma H_T sample ($N = 20$) contains only 11 galaxies to which T is available. The error of $m - M$ is given in parentheses.

REFERENCES

Aaronson, M. 1977, Ph.D. thesis, Harvard University.

Aaronson, M., Bothun, G., Mould, J., Huchra, J., Schommer, R. A., Cornell, M. E. 1986, ApJ, 302, 536

Aaronson, M., et al. 1989, ApJ, 338, 654

Aaronson, M., Huchra, J., Mould, J. 1979, ApJ, 229, 1

Aaronson, M., Huchra, J., Mould, J., Tully, R. B., Fisher, J. R., van Woerden, H., Goss, W. M., Chamaraux, P., Mebold, U., Siegman, B., Berriman, G., Persson, S. E. 1982, ApJS, 50, 241

Bernstein, G. M., Guhathakurta, P., Raychaudhury, S., Giovanelli, R., Haynes, M. P., Herter, T., Vogt, N. P. 1994, AJ, 107, 1962

Bothun, G. D., Aaronson, M., Schommer, B., Mould, J., Huchra, J., Sullivan, W. T. 1985, ApJS, 57, 423

Burstein, D., Heiles, C. 1984, ApJS, 54, 33

Elias, J. H., Frogel, J. A., Matthews, K., Neugebauer, G. 1982, AJ, 87, 1029

Epchtein N., et al. 1994, Ap & Space Sci., 217, 3

Ferrarese, L., et al. 1998, ApJ, 507, 655

Freedman, W. L. 1990, ApJ, 355, L35

Giovanelli, R., Haynes, M. P., Herter, T., Vogt, N. P., Wegner, G., Salzer, J. J., da Costa, L. N., Freudling, W. 1997a, AJ, 113, 22

Giovanelli, R., Haynes, M. P., Herter, T., Vogt, N. P., da Costa, L. N., Freudling, W., Salzer, J. J., Wegner, G. 1997b, AJ, 113, 53

Gibson, B. K., et al. 1999, ApJ, 512, 48

Graham, J. A., et al. 1997, ApJ, 477, 535

Glass, I. S. 1976, MNRAS, 175, 191

Han, M. 1992, ApJ, 391, 617

Huchtmeier, W. K., Richter, O. G. 1989 *A General Catalog of HI Observations of Galaxies* (New York: Springer-Verlag)

Hughes, S. M. G., et al. 1998, ApJ, 501, 32

Itoh, N., Yanagisawa, K., Ichikawa, T. 1995, in Proc. of SPIE Vol.2552, Infrared Technology, eds. B. F. Andresen & M. S. Scholl (Washington: SPIE), 430

Kelson, D. D., et al. 1999, ApJ, 514, 614

Macri, L. M., et al. 1999, ApJ, 521, 155

McGaugh, S. S., Schombert, J. M., Bothun, G. D., de Blok, W. J. G. 2000, ApJ, 533, L99

Mould, J., Han, M., Bothun, G. 1989, ApJ, 347, 112

Peletier, R. F., Willner, S. P. 1991, ApJ, 382, 382

Peletier, R. F., Willner, S. P. 1993, ApJ, 418, 626

Pierce, M. J., Tully, R. B. 1988, ApJ, 330, 579

Saha, A., Sandage, A., Labhardt, L, Tammann, G. A., Macchetto, F. D., Panagia, N. 1996, ApJ, 466, 55

Saha, A., Sandage, A., Labhardt, L, Tammann, G. A., Macchetto, F. D., Panagia, N. 1997, ApJ, 486, 1

Sakai, S., et al. 1999, ApJ, 523, 540

Sakai, S., et al. 2000, ApJ, 529, 698

Schlegel, D. J., Finkbeiner, D. P., Davis, M. 1998, ApJ, 500, 525

Silbermann, N. A., et al. 1996, ApJ, 470, 1

Skrutskie, M. F., et al. 1997, in The Impact of Large Scale Near-IR Sky Surveys, eds. F. Garzon et al. (Dordrecht: Kluwer), 25.

Tanvir, N. R., Shanks, T., Ferguson, H. C., Robinson, D. R. T. 1995, Nature, 377, 27

Tormen, G., Burstein, D. 1995, ApJS, 96, 123

Tully, R. B., Pierce, M. J., Huang, J., Saunders, W., Verheijin M. A. W., Witchalls, P. L. 1998, AJ, 115, 2265

Turner, A., et al. 1998, ApJ, 505, 207

de Vaucouleurs, G., de Vaucouleurs, A., Corwin, Jr., H. G., Buta, R. J., Paturel, G., Fouqué, P. 1991, *Third Reference Catalogue of Bright Galaxies* (New York: Springer-Verlag) (RC3)

Yanagisawa, K., Itoh, N., Ichikawa, T. 1996, in Proc. of SPIE Vol.2744, Infrared Technology and Applications XXII, eds. B. F. Andresen & M. S. Scholl (Washington: SPIE), 92

Fig. 1.— The luminosity profile (upper panel) and contour maps in J (lower left) and H (lower right) for the nearby calibrator galaxies. The profiles denoted by triangles and squares are for J and H, respectively. Error bars represents only the isophote fitting error. R.A. and Dec in the maps are given in arcmin with an arbitrary zero point. The interval of the contours is $0.5\,\mathrm{mag\,arcsec^{-2}}$. The faintest contour levels displayed are $\mu_J = 22\,\mathrm{mag\,arcsec^{-2}}$ and $\mu_H = 21\,\mathrm{mag\,arcsec^{-2}}$. Some foreground stars are removed, but they are not necessarily identical between J and H images. See text for possibly disturbed isophotes of the J image of NGC 925.

Fig. 2.— Comparison between our growth curve (solid curve) and the aperture photometry data given in the literature (open squares). Both J and H data are displayed where available. A dotted line and a filled square show the template curve and the resultant $H_{-0.5}$ adopted by TB95, respectively, except for NGC 4639 for which $H_{-0.5}$ is not given and the template curve is displayed with arbitrary zero point.

Fig. 3.— Calibration of IRTFs for H_T, $H_{-0.5}$, H_{21}, H_{19}, J_T, and J_{22}.

Fig. 4.— A luminosity offset $H^s_{-0.5} - H_T$ plotted against the axial ratio D_{min}/D_{maj} for the nearby calibrators, Coma and UMa galaxies. Early spirals with $T \leq 4$ are shown by circles while late spirals with $T \geq 5$ are shown by squares.

Fig. 5.— A color $(I - H)_T$ plotted against $\log W^c_{20}$ for the nearby calibrators (filled squares), Coma galaxies (stars) and Ursa Major galaxies (circles).

Fig. 6.— The same as Fig.5 but for $(B - H)_T$.

Fig. 7.— H-band IRTF diagrams for the Ursa Major galaxies (small squares) overplotted by the nearby calibrators (large squares). A small open square represents NGC 3718 (see section 5.4 for detail). The calibrators are vertically scaled according to the best estimates of the cluster distance modulus. The H magnitudes used are, from the left panel to right, H_T, $H_{-0.5}$, and H_{19}.

Fig. 8.— The same as Fig.7 but for the Coma galaxies. The H magnitudes used are H_T (the left and middle panels) and $H_{-0.5}$ (the right panel). In the left panel the distance is estimated using all the Coma galaxies including those without $H_{-0.5}$ data (crosses). In the middle panel, on the other hand, the distance is estimated just using those with $H_{-0.5}$ data.

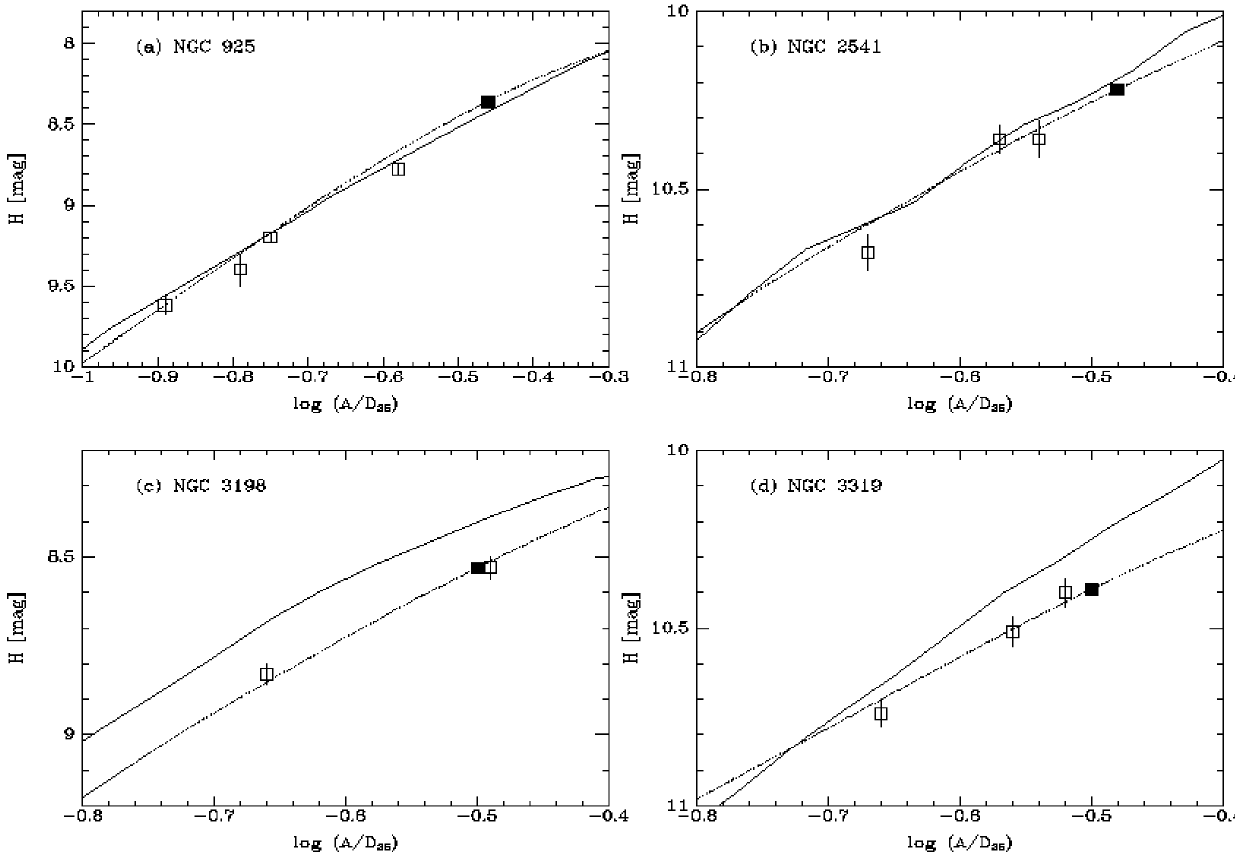

(a) NGC 925
(b) NGC 2541
(c) NGC 3198
(d) NGC 3319
H [mag]
log (A/D25)

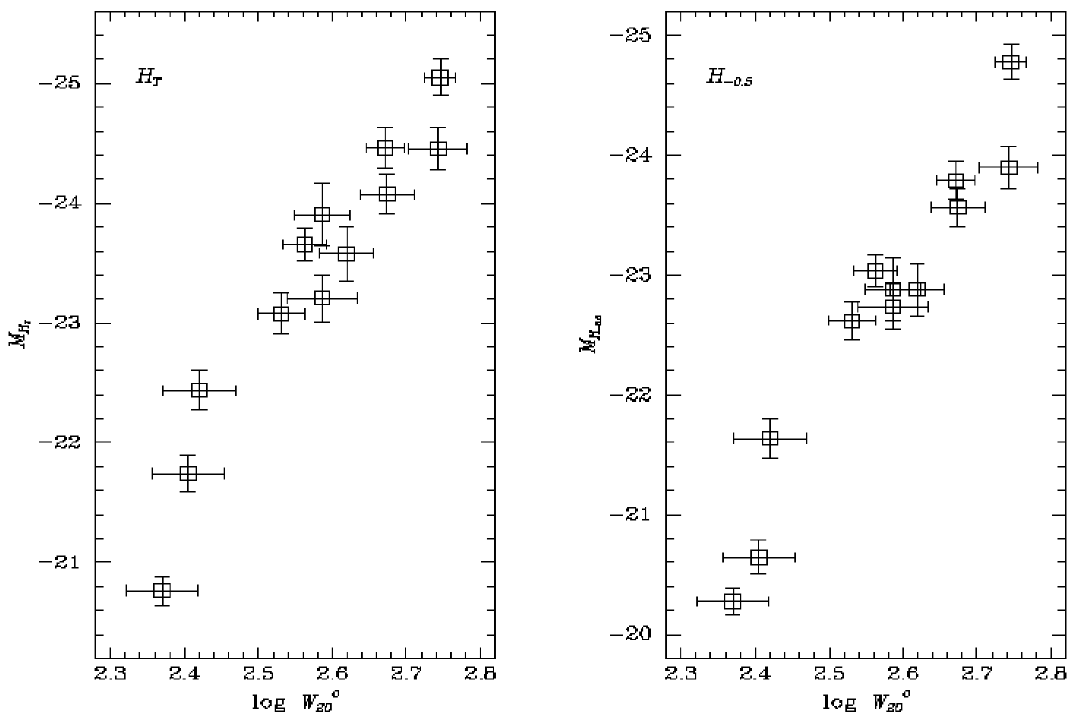

H_T
M_{H_T}
−25
−24
−23
−22
−21
2.3
2.4
2.5
2.6
2.7
2.8
log $W_{20}{}^{c}$
$H_{-0.5}$
$M_{H_{-0.5}}$
−25
−24
−23
−22
−21
−20
2.3
2.4
2.5
2.6
2.7
2.8
log $W_{20}{}^{c}$

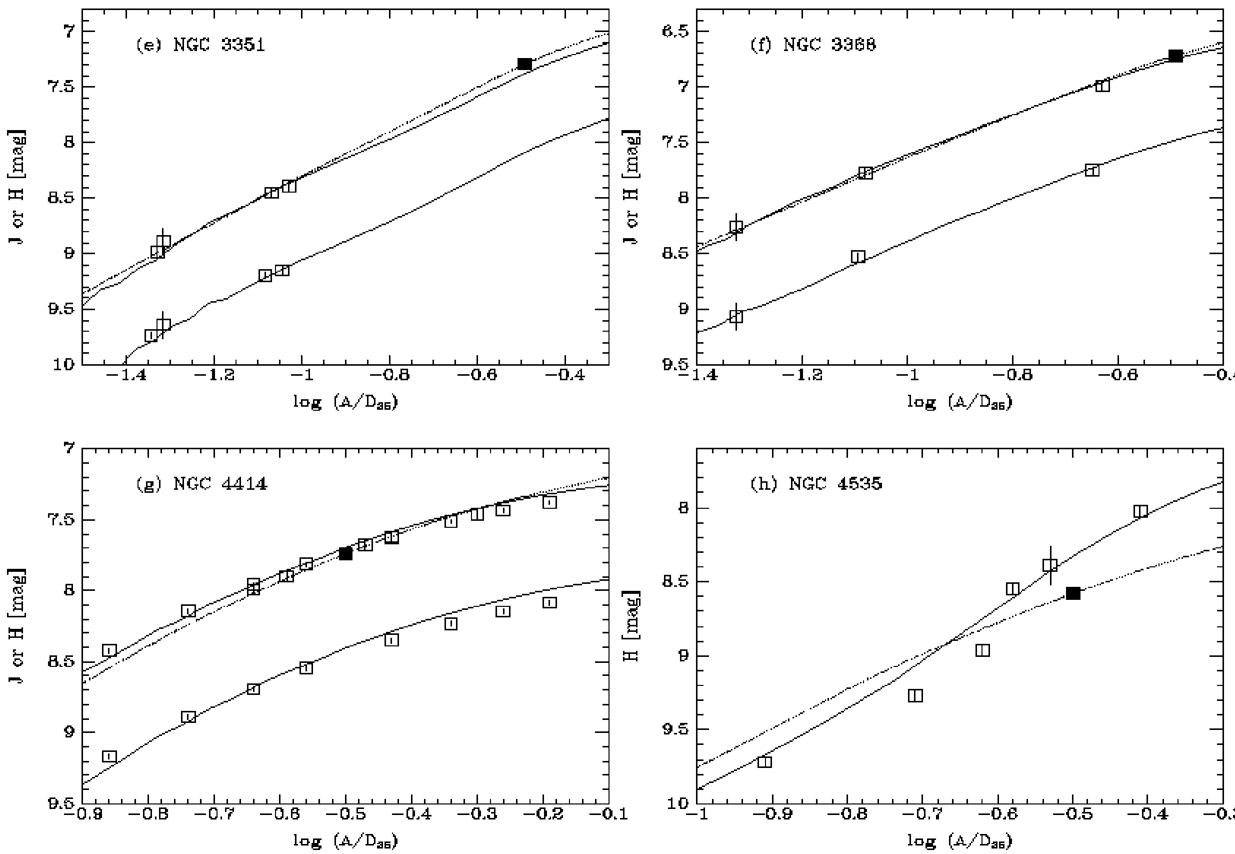

(e) NGC 3351
(f) NGC 3368
(g) NGC 4414
(h) NGC 4535
J or H [mag]
H [mag]
log (A/D$_{25}$)

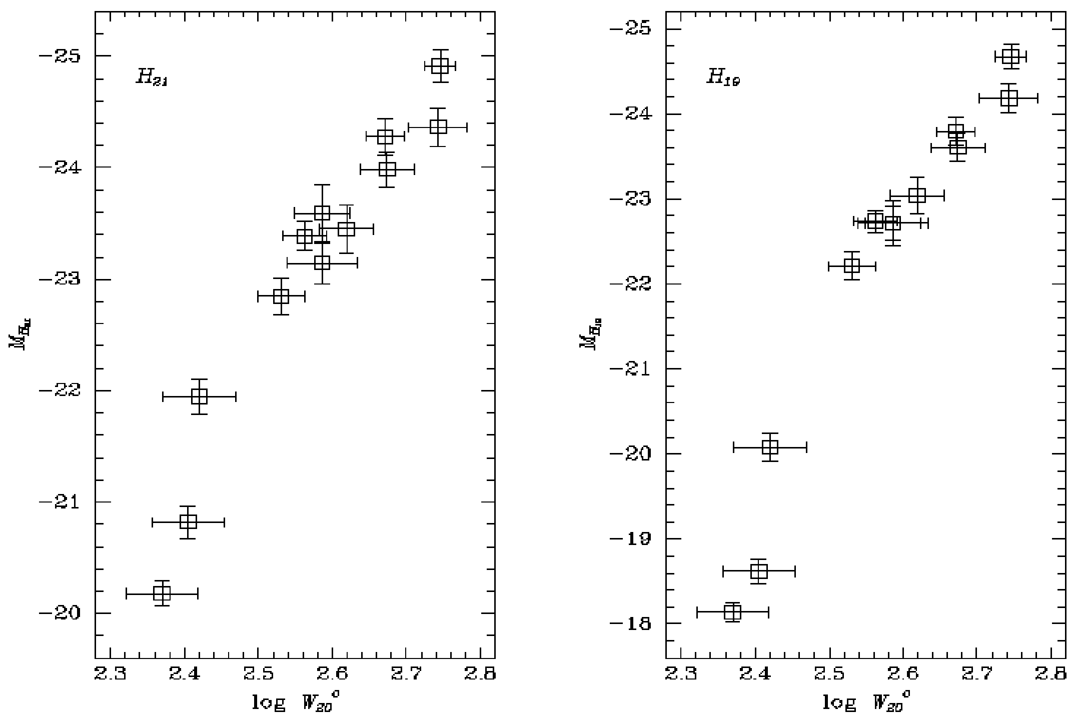

H21
$M_{H_{21}}$
log W_{20}^{c}
-25
-24
-23
-22
-21
-20
2.3
2.4
2.5
2.6
2.7
2.8
H19
$M_{H_{19}}$
log W_{20}^{c}
-25
-24
-23
-22
-21
-20
-19
-18
2.3
2.4
2.5
2.6
2.7
2.8

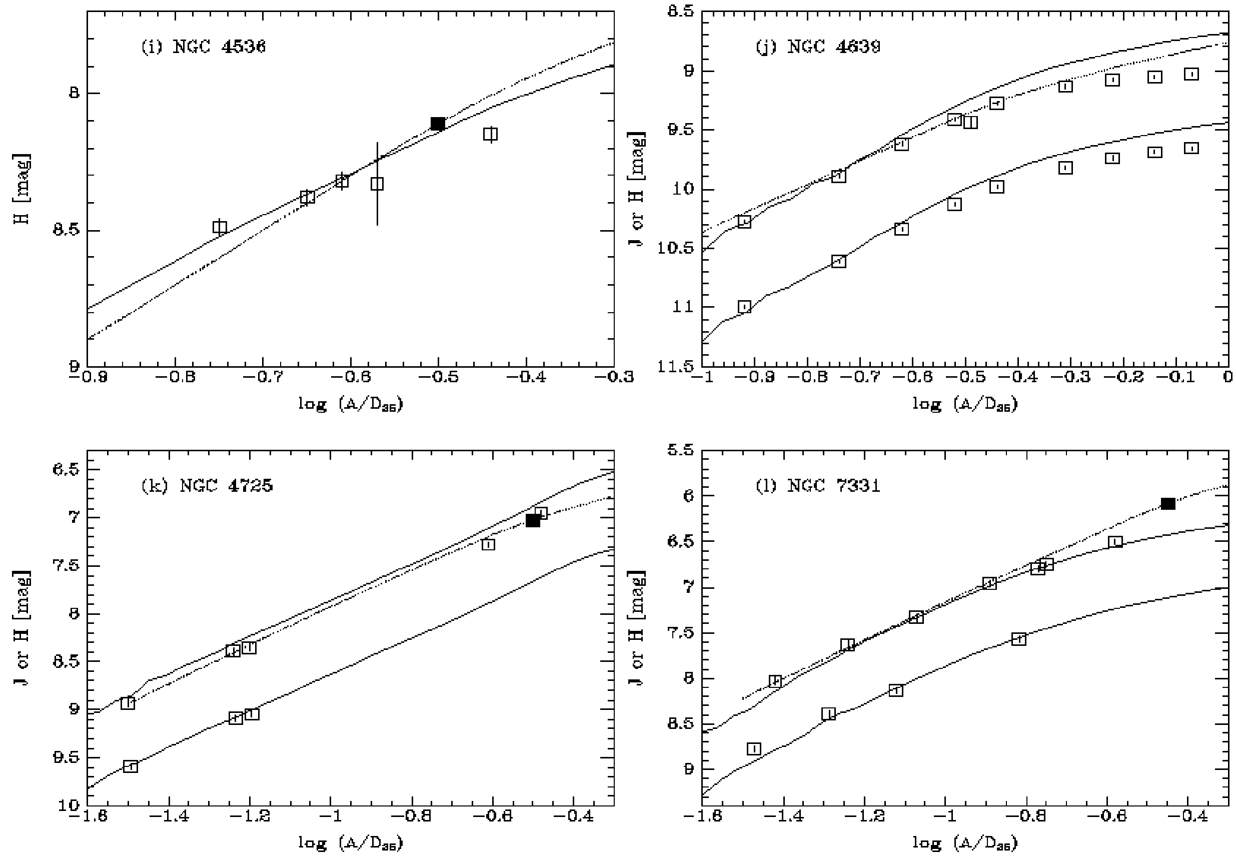

(i) NGC 4536
H [mag]
log (A/D25)
(j) NGC 4639
J or H [mag]
log (A/D25)
(k) NGC 4725
J or H [mag]
log (A/D25)
(l) NGC 7331
J or H [mag]
log (A/D25)

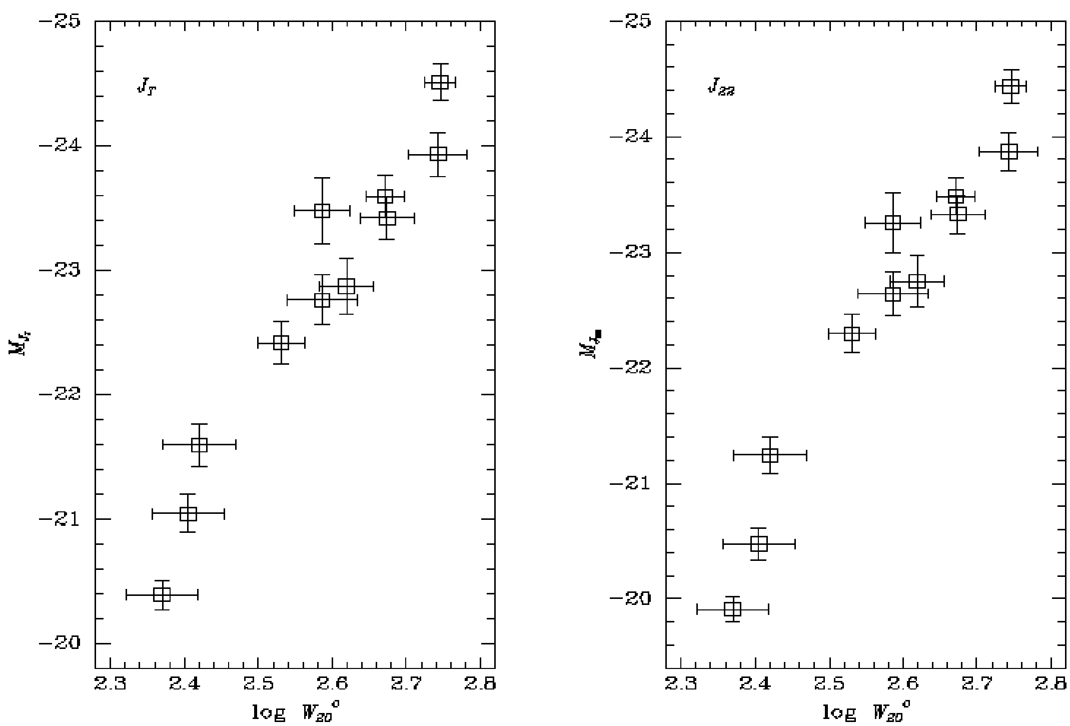

J_T
M_{J_T}
log $W_{20}^{\,c}$
J_{22}
$M_{J_{22}}$
log $W_{20}^{\,c}$

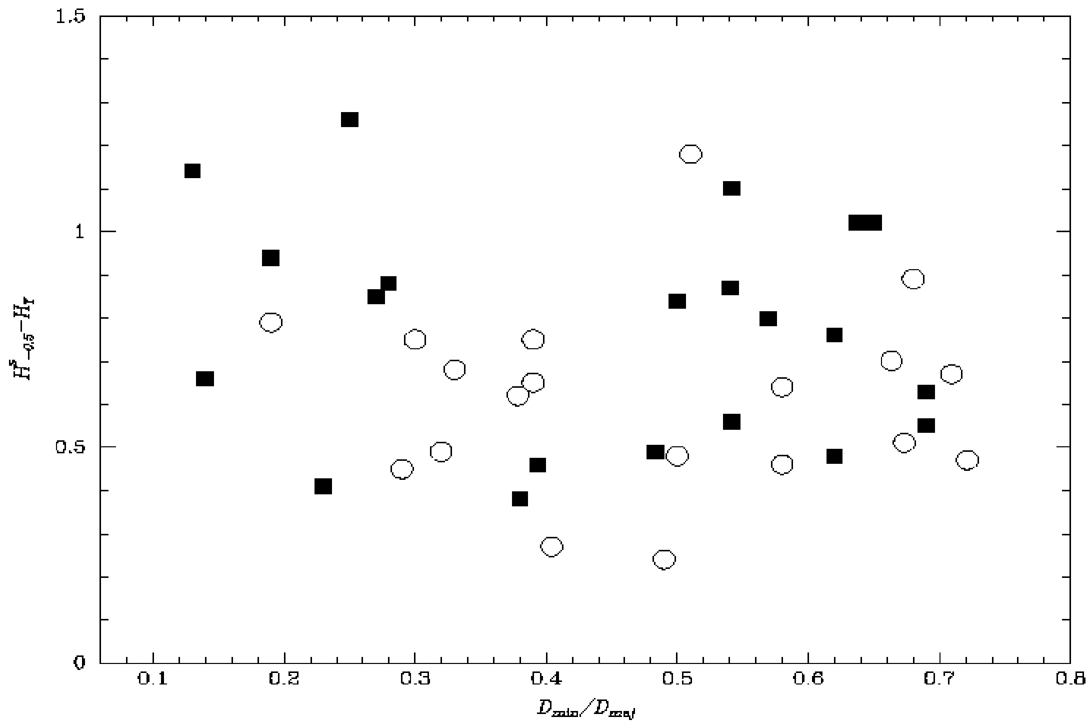

1.5
1
0.5
0
0.1
0.2
0.3
0.4
0.5
0.6
0.7
0.8
$H^s_{-0.5}-H_T$
D_{min}/D_{maj}

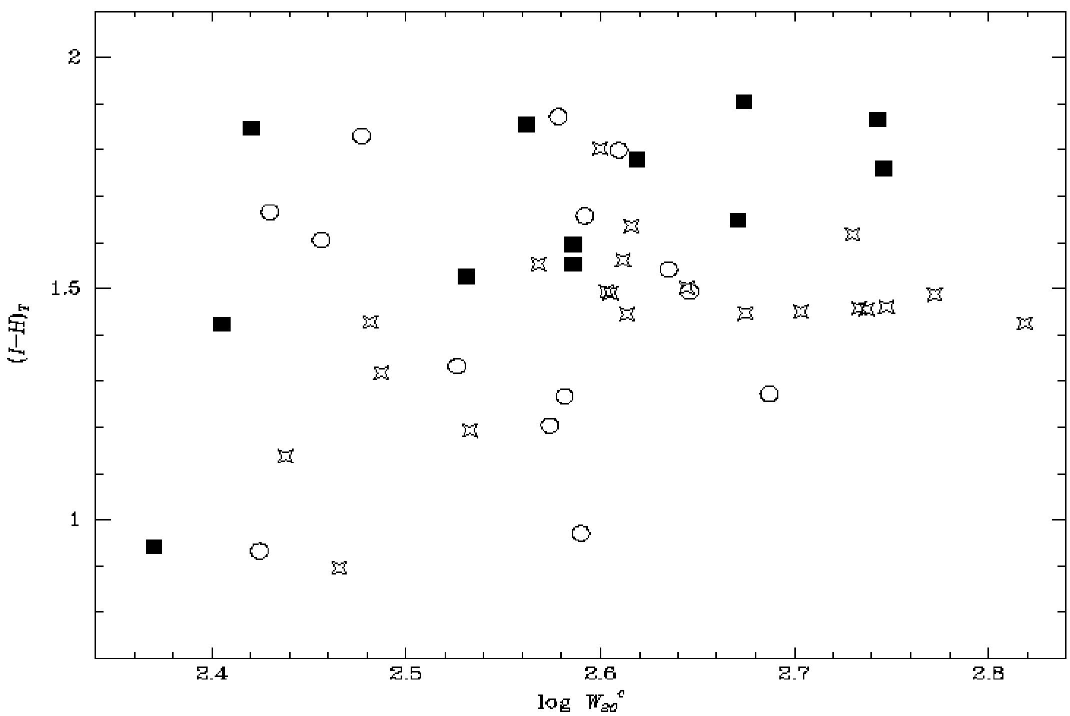

2
1.5
1
2.4
2.5
2.6
2.7
2.8
(I−H)T
log W20c

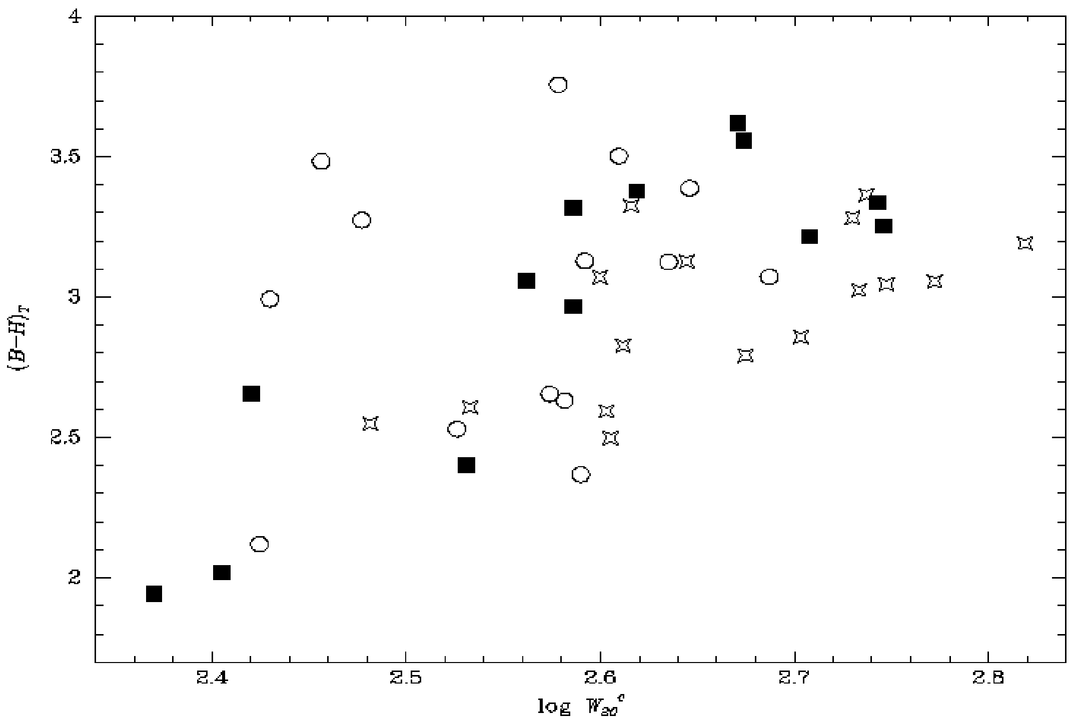

4
3.5
3
2.5
2
2.4
2.5
2.6
2.7
2.8
$(B-H)_T$
log W_{20}^c

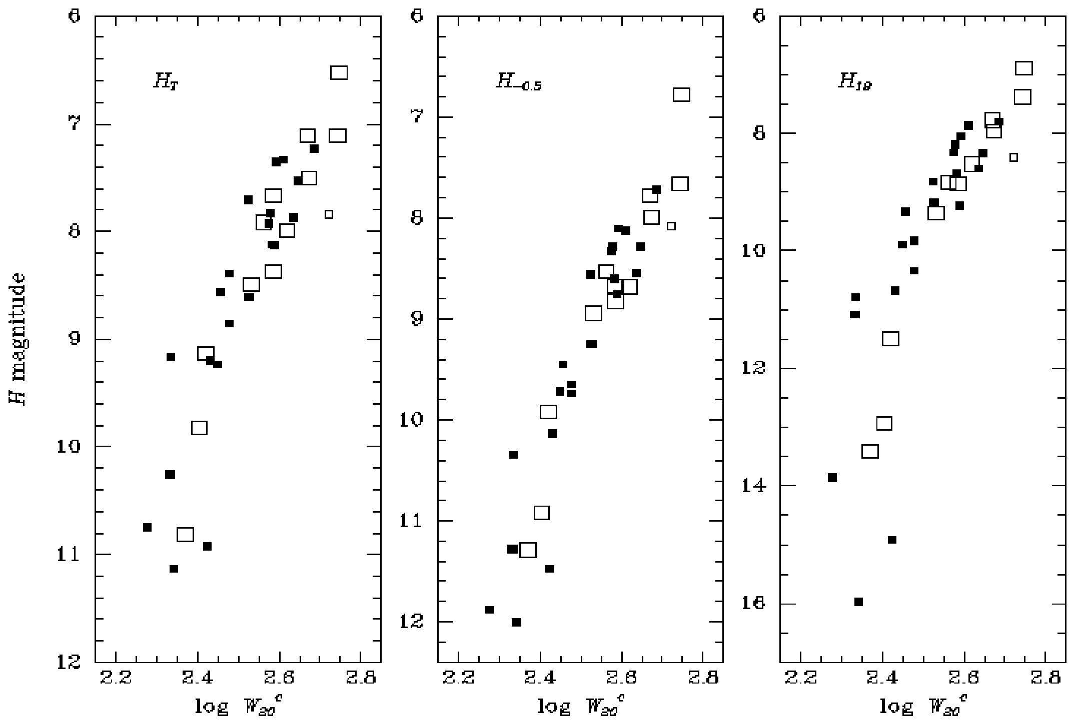

H_T
$H_{-0.5}$
H_{19}
H magnitude
log W_{20}^c
log W_{20}^c
log W_{20}^c

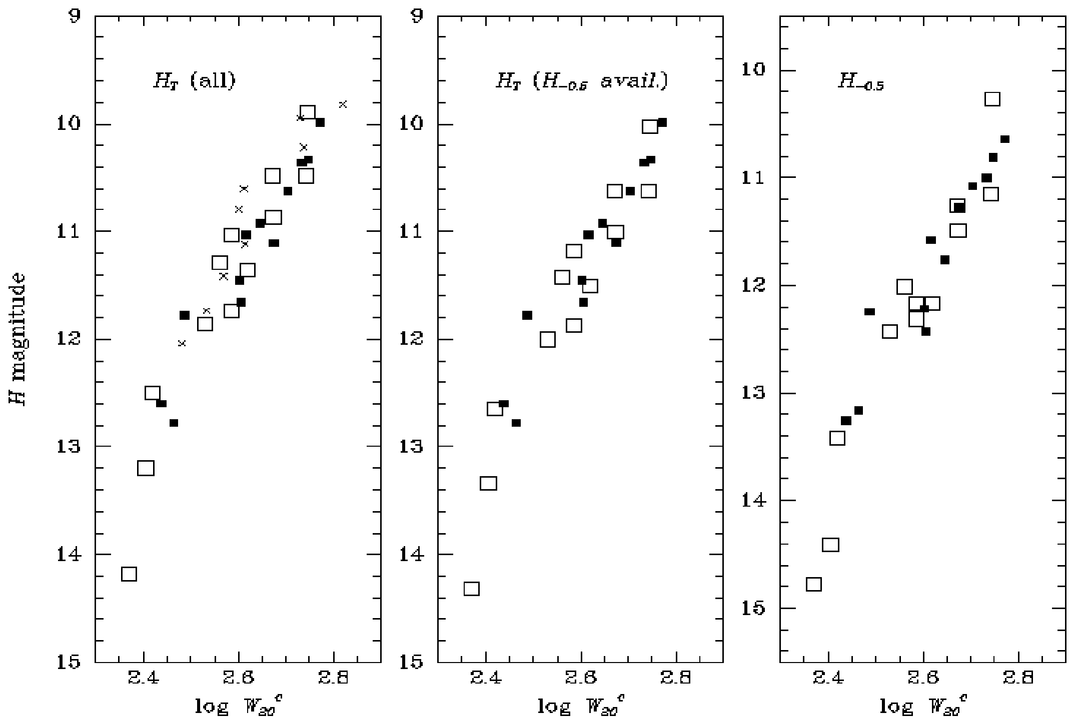

H_T (all)
H_T ($H_{-0.5}$ avail.)
$H_{-0.5}$
H magnitude
log W_{20}^c
log W_{20}^c
log W_{20}^c
9
10
11
12
13
14
15
2.4
2.6
2.8

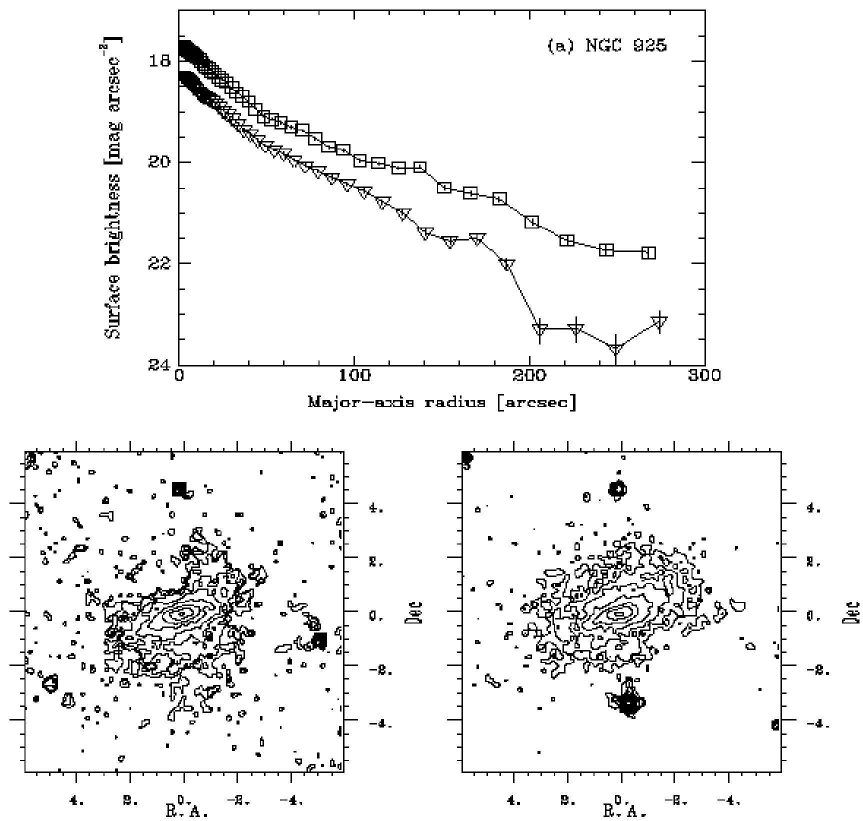

(a) NGC 925
Surface brightness [mag arcsec^{-2}]
Major-axis radius [arcsec]
18
20
22
24
0
100
200
300
R.A.
Dec
4.
2.
0.
-2.
-4.

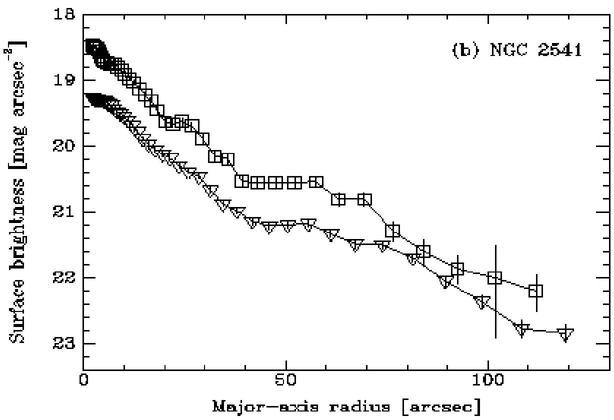
(b) NGC 2541
Surface brightness [mag arcsec^{-2}]
Major-axis radius [arcsec]
18
19
20
21
22
23
0
50
100

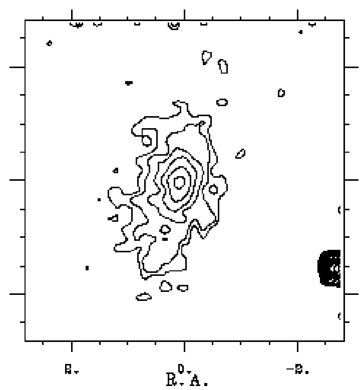
R.A.
Dec
2.
0.
-2.

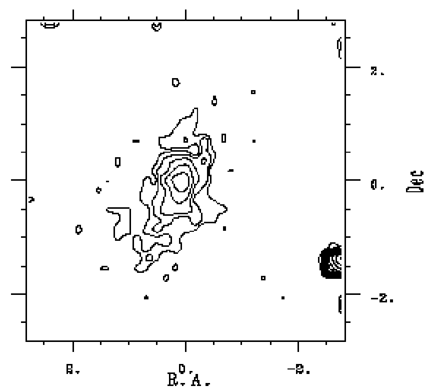
R.A.
Dec
2.
0.
-2.

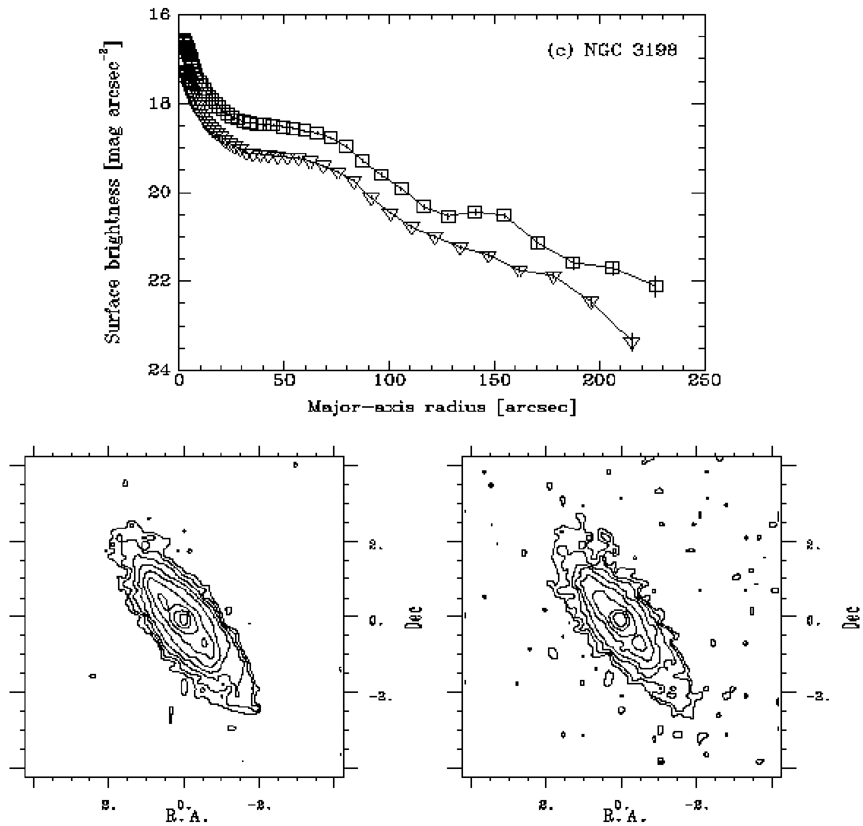

(c) NGC 3198
Surface brightness [mag arcsec^{-2}]
Major-axis radius [arcsec]
16
18
20
22
24
0
50
100
150
200
250
R.A.
Dec
2.
0.
-2.

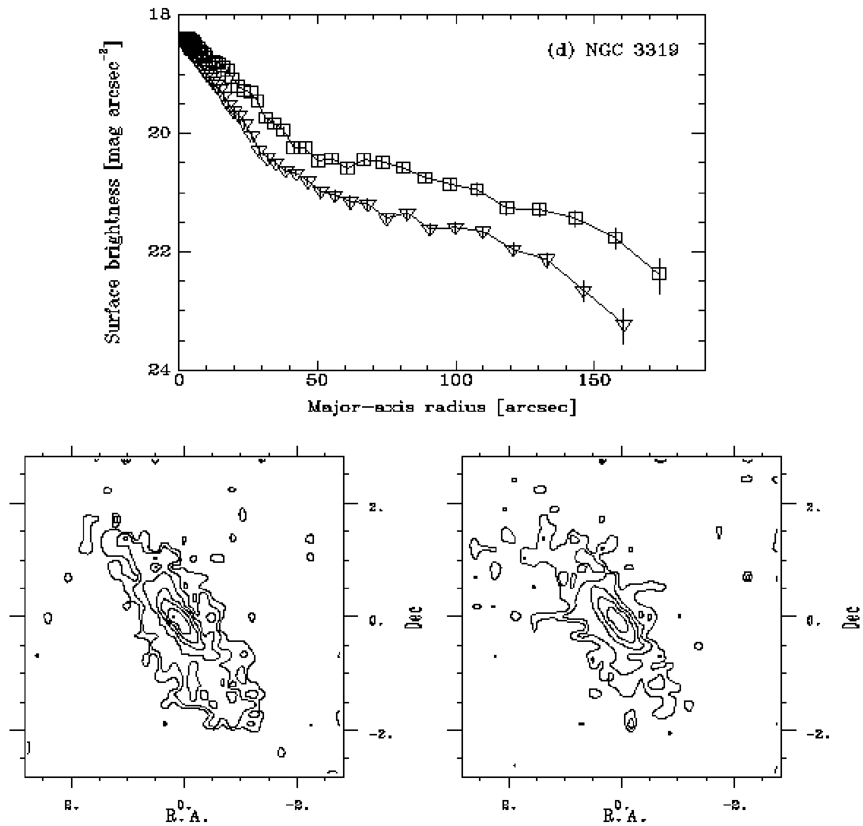
(d) NGC 3319
Surface brightness [mag arcsec^{-2}]
Major-axis radius [arcsec]
18
20
22
24
0
50
100
150
2.
0.
-2.
Dec
R.A.
2.
0.
-2.
Dec
R.A.

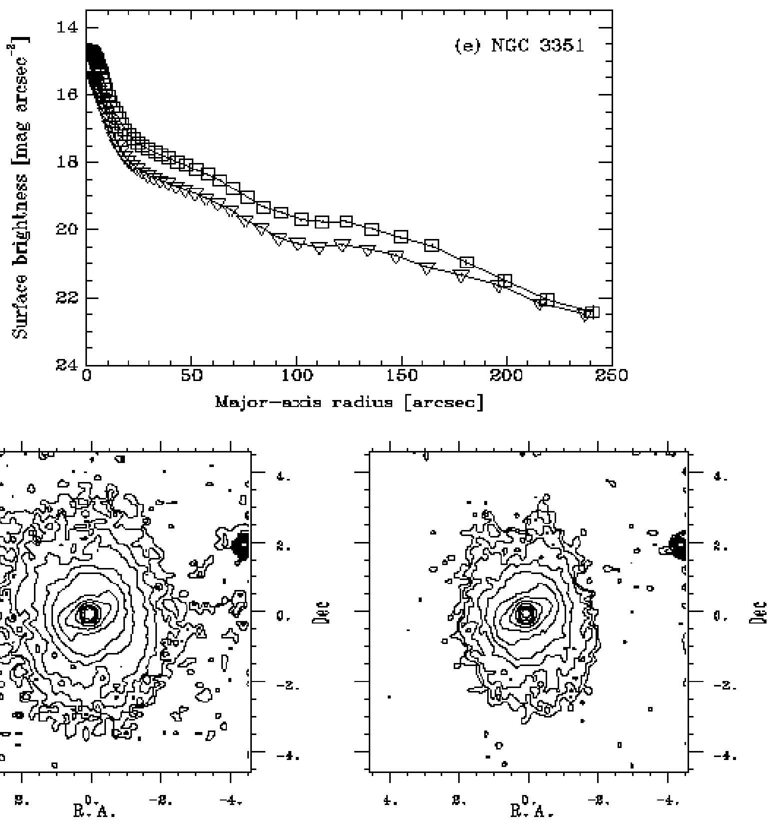

(e) NGC 3351
Surface brightness [mag arcsec^{-2}]
Major-axis radius [arcsec]
R.A.
Dec

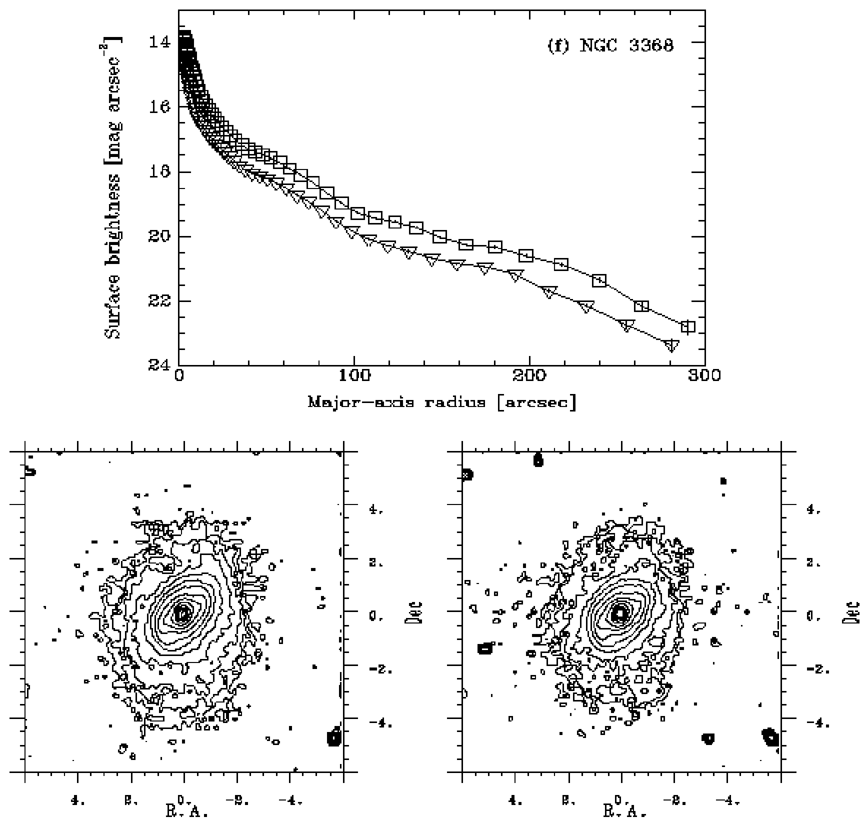

(f) NGC 3368
Surface brightness [mag arcsec^{-2}]
Major-axis radius [arcsec]
R.A.
Dec
R.A.
Dec

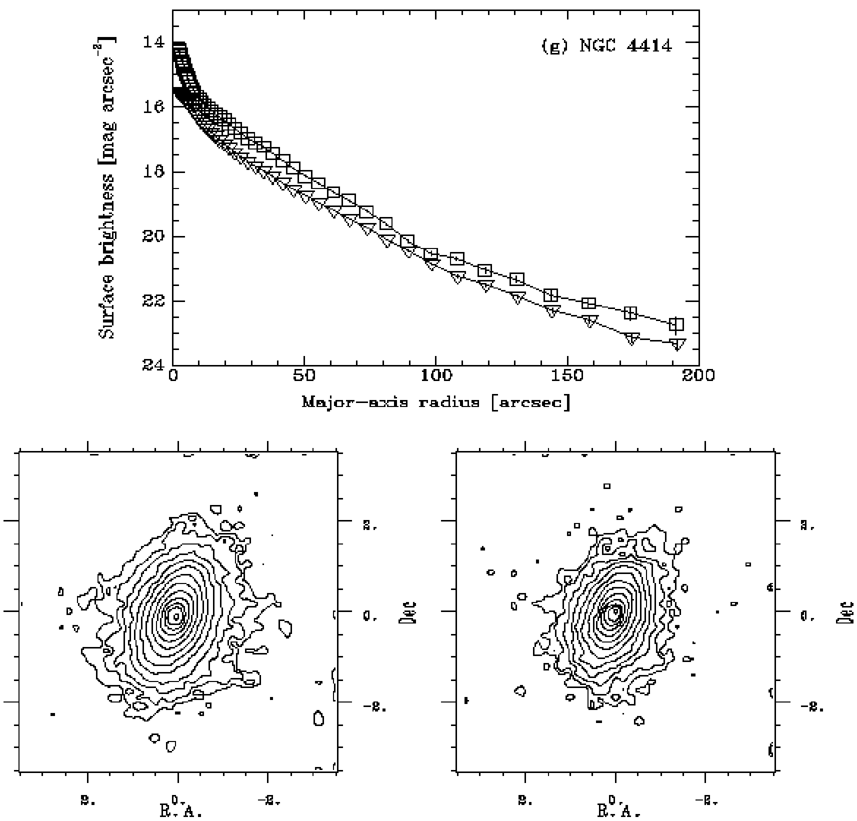
(g) NGC 4414
Surface brightness [mag arcsec^{-2}]
Major-axis radius [arcsec]
R.A.
Dec

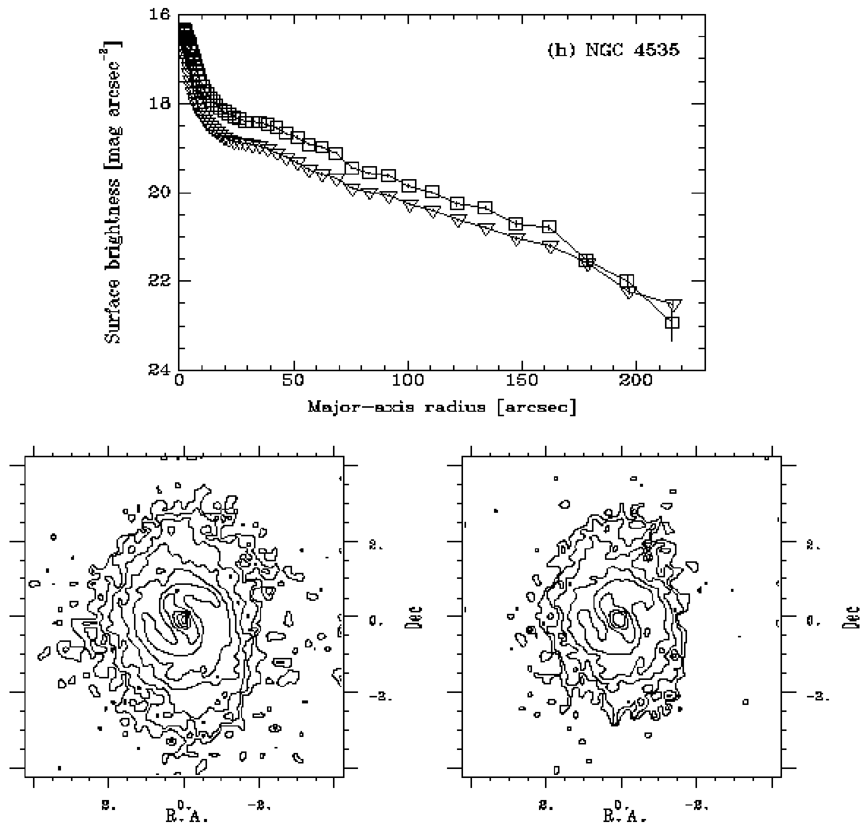

(h) NGC 4535
Surface brightness [mag arcsec^{-2}]
Major-axis radius [arcsec]
R.A.
Dec

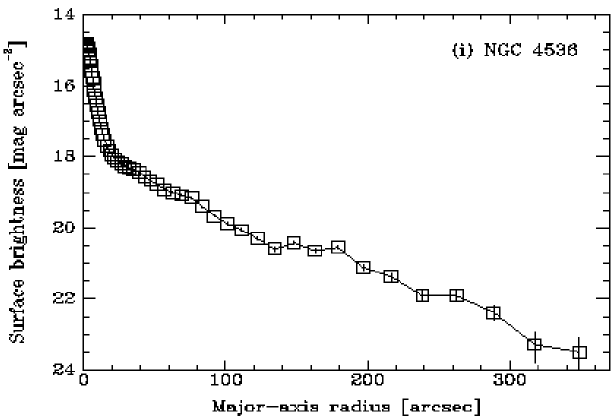
(i) NGC 4536
Surface brightness [mag arcsec^{-2}]
Major-axis radius [arcsec]
14
16
18
20
22
24
0
100
200
300

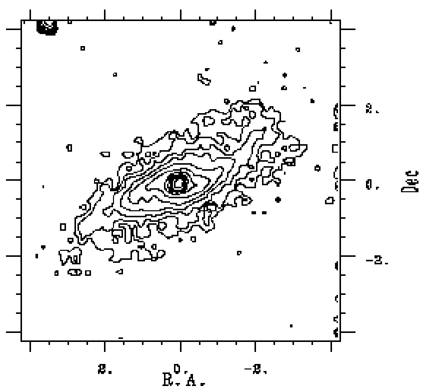
Dec
R.A.

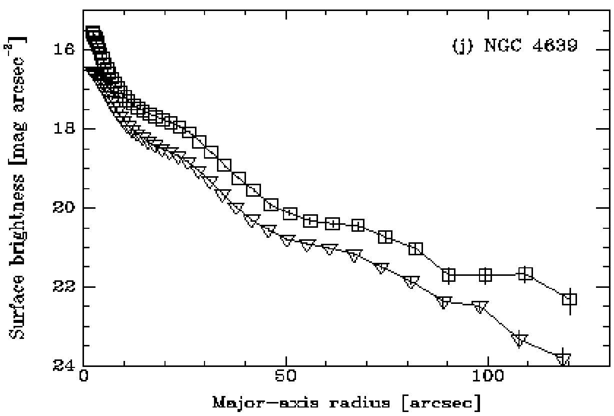
(j) NGC 4639
Surface brightness [mag arcsec^{-2}]
Major-axis radius [arcsec]
16
18
20
22
24
0
50
100

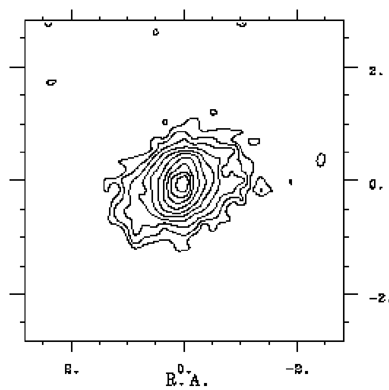
2.
0.
-2.
Dec
R.A.

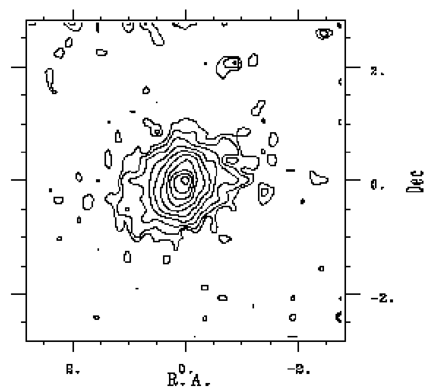
2.
0.
-2.
Dec
R.A.

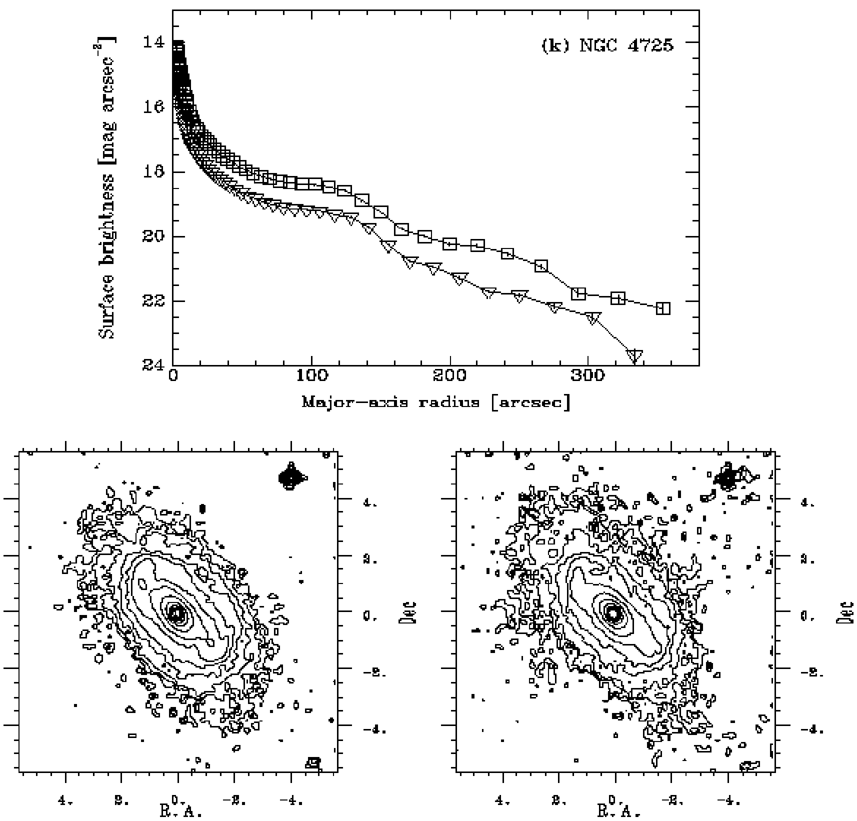
(k) NGC 4725
Surface brightness [mag arcsec^{-2}]
Major-axis radius [arcsec]
R.A.
Dec
R.A.
Dec

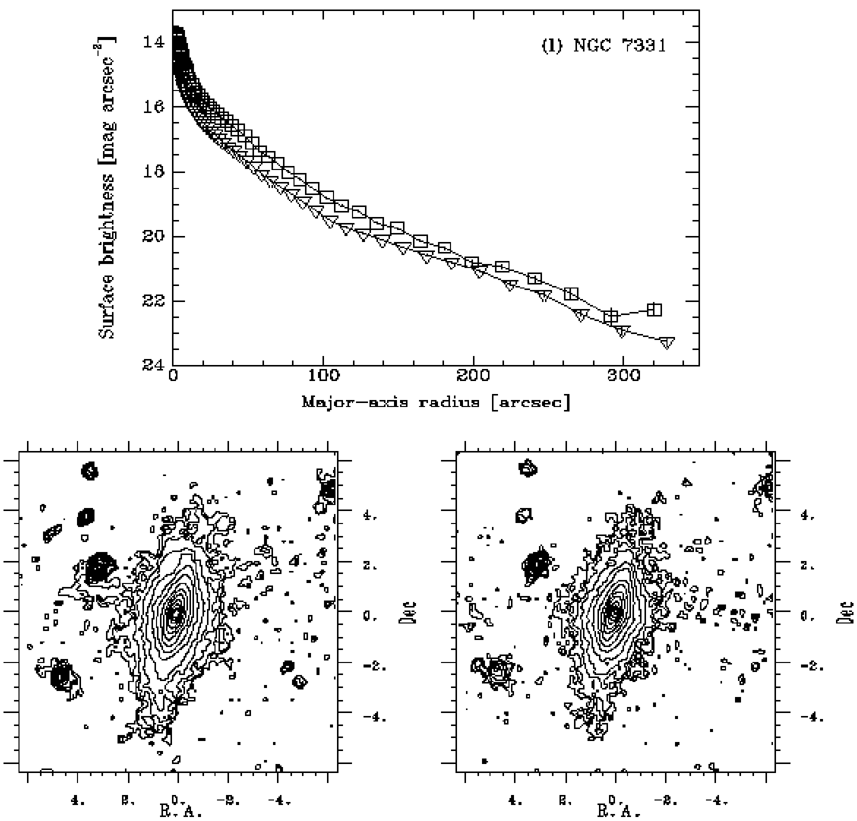
(I) NGC 7331
Surface brightness [mag arcsec^-2]
Major-axis radius [arcsec]
R.A.
Dec
R.A.
Dec